Universidade Federal do Rio de Janeiro

USO DO MÉTODO S_{PB} COM USO DE DIGITAL IMAGE CORRELATION (DIC) PARA AVALIAÇÃO DA TENACIDADE À FRATURA DE PVDF

Lucas Kenji Ychisawa

2019

Universidade Federal do Rio de Janeiro
Escola Politécnica

USO DO MÉTODO S_{PB} COM USO DE DIGITAL IMAGE CORRELATION (DIC) PARA AVALIAÇÃO DA TENACIDADE À FRATURA DE PVDF

Lucas Kenji Ychisawa

Projeto de Graduação apresentado ao Curso de Engenharia de Materiais da Escola Politécnica, Universidade Federal do Rio de Janeiro, como parte dos requisitos necessários à obtenção do título de Engenheiro.

Orientador: Celio Albano da Costa Neto

Rio de Janeiro

Janeiro de 2019

THE USE OF S_{PB} METHOD WITH THE AID OF DIGITAL IMAGE CORRELATION (DIC) TO EVALUATE THE FRACTURE TOUGHNESS OF PVDF

Lucas Kenji Ychisawa

PROJETO DE GRADUAÇÃO SUBMETIDO AO CORPO DOCENTE DO CURSO DE ENGENHARIA DE MATERIAIS DA ESCOLA POLITÉCNICA DA UNIVERSIDADE FEDERAL DO RIO DE JANEIRO COMO PARTE DOS REQUISITOS NECESSÁRIOS PARA A OBTENÇÃO DO GRAU DE ENGENHEIRO DE MATERIAIS.

Examinado por:

Prof. Celio Albano da Costa Neto, Ph.D.

Profª. Marysilvia Ferreira da Costa, D. Sc.

Eng. Egon Rolf Delgado Ramirez, M. Sc.

Eng. Nara Guidacci Berry, D. Sc.

Rio de Janeiro, RJ – Brasil

Janeiro de 2019

Ychisawa, Lucas Kenji

Uso do Método S_{pb} com uso de DIC para Avaliação da Tenacidade à Fratura de PVDF/ Lucas Kenji Ychisawa. – Rio de Janeiro: UFRJ/ Escola Politécnica, 2019

VIII, 61 p.: il.;29.7cm

Orientador: Celio Albano da Costa Neto

Projeto de Graduação – UFRJ/ Escola Politécnica/ Curso de Engenhariad e Materiais, 2019.

Referências Bibliográficas: p. 48-49

1. PVDF. 2. Mecânica da Fratura. 3. Digital Image Correlation. 4. S_{pb}. 5. Polímeros. I. Costa Neto, Celio Albano da. II. Universidade Federal do Rio de Janeiro, UFRJ, Curso de Engenharia de Materiais. III. Uso do Método S_{pb} com uso de Digital Image Correlation (DIC) para Avaliação da Tenacidade à Fratura de PVDF.

Agradecimentos

Gostaria de agradecer primeiramente a minha família por sempre me apoiar em todos os momentos da minha vida e possibilitar dedicação integral a formação, em especial a minha mãe, Cristiane Sayuri Ota, e ao meu pai do coração, Marcio Pereira Rippel.

Ao meu orientador, Celio Costa, por sempre ter me apoiado e acreditado no meu potencial, além de todo o conhecimento transmitido. Tudo isso foi de grande importância para o meu crescimento, tanto acadêmico quanto pessoal.

À toda equipe do Laboratório de Processamento e Caracterização de Materiais pelos ensinamentos e atividades ao longo dos dias no laboratório. Destaco o apoio e companheirismo de Rafael Luis e Antônio Pedro, sempre presentes nos diversos ensaios.

À equipe do Laboratório de Mecânica de Fratura, em especial a Egon Delgado, por apresentar o método S_{pb} explorado nesse trabalho, assim como por auxiliar em ensaios de fratura e estar sempre disponível para tirar qualquer dúvida.

À equipe do CENPES que permitiu e auxiliou na análise de MEV neste trabalho.

À UFRJ, por me proporcionar a oportunidade de realizar o curso de Engenharia de Materiais, e de me aprimorar profissional e pessoalmente.

Resumo do Projeto de Graduação apresentado à Escola Politécnica/ UFRJ como parte dos requisitos necessários para a obtenção do grau de Engenheiro de Materiais.

USO DO MÉTODO S_{PB} COM USO DE DIGITAL IMAGE CORRELATION (DIC) PARA AVALIAÇÃO DA TENACIDADE À FRATURA DE PVDF

Lucas Kenji Ychisawa

Janeiro/2019

Orientador: Celio Albano da Costa Neto, Ph.D.

Curso: Engenharia de Materiais

O Polifluoreto de Vinilideno, ou PVDF, é muito utilizado na indústria de óleo e gás devido a sua capacidade de suportar altas temperaturas de trabalho, enquanto apresenta propriedades mecânicas e químicas superiores à diversos polímeros termoplásticos. Quando lidamos com aplicações estruturais como esta, é de grande importância o estudo de suas propriedades mecânicas sob condições de teste semelhantes às condições de trabalho. O objetivo desse trabalho foi estudar a possibilidade de aplicação do método S_{pb}, que possibilita a determinação do início da propagação de uma trinca a partir da medida de carga, junto do uso do DIC, uma técnica de medição de deformação a partir de uma série de imagens do ensaio, bem como utilizar esse método para comparar a tenacidade à fratura de dois grades comerciais de PVDF e para estudar o efeito do envelhecimento sob as propriedades de fratura do material. O material foi caracterizado por meio de ensaios de DSC e ensaios mecânicos, tanto ensaio tração quanto ensaios de fratura. Ao final, conclui-se que o método pode ser utilizado para ambos os grades de PVDF se o ensaio de fratura for realizado com uma velocidade do travessão de 10 mm/min e que um aumento na cristalinidade leva a uma maior tenacidade à fratura, porém a fratura ocorre a menores deformações.

Palavras-chave: PVDF, Mecânica da Fratura, DIC, S_{pb}, Polímeros.

Abstract of Undergraduate Project presented to POLI/UFRJ as a partial fulfillment of the requirements for the degree of Materials Engineer.

THE USE OF S_{PB} METHOD WITH THE AID OF DIGITAL IMAGE CORRELATION (DIC) TO EVALUATE THE FRACTURE TOUGHNESS OF PVDF

Lucas Kenji Ychisawa

January/2019

Advisor: Celio Albano da Costa Neto, Ph.D.

Course: Materials Engineering

Polyvinylidene Fluoride is often used in the oil and gas industry due to its ability to withstand high working temperatures, as well as to its mechanical and chemical properties, which are superior to most thermoplastics. When studying structural application such as this, it is of great importance the ability to study the material's mechanical properties under test conditions similar to the working conditions. The objective of this work was to evaluate the use of the S_{PB} method, which is a methodology able to determine the beginning of the crack propagation through load measurement, with the PVDF while also using DIC, which is a method to determine displacement fields and deformation fields in a specimen's surface through a series of images taken during the test. These methods were used to compare the fracture properties of two commercial grades of PVDF and to study the effects of annealing in the fracture toughness. The materials were characterized through DSC and mechanical tests, such as tensile tests and fracture tests. In the end of the study, it was concluded that the S_{PB} method can be applied to both grades of PVDF if the fracture test is done with a crosshead of 10 mm/min and that an increase in crystallinity leads to an increase in fracture toughness, but also a decrease in the displacement required to cause crack propagation.

Table of Contents

1. Introduction

Polymeric materials nowadays are widely used in many different areas, from housewares and toys to coatings and structural applications in the oil and gas industry. This is due to their low density, easy processing and large range of properties, which make them really versatile.

The origin of the polymer industry was in the beginning of the 19th century when in 1839 Charles Goodyear found that the properties of the natural rubber could be changed and improved by heating it with Sulphur, a process that came to be known as vulcanization. Some years later, cellulose nitrate was developed and it was observed that it was soluble and it could be molded by applying and pressure. Up to this point, all polymers were made from natural polymers, in other words, there were either natural or semi-synthetic. However, this changed in the 20th century, when the structure of polymers was better understood and its structure composed of large chains was widely known and accepted, which was displayed by the creation of the Bakelite. This allowed for new and more advanced polymers, such as Nylon, PVC, etc. to me manufactured [1].

Since this type of material is seeing increasing use, especially in structural applications, the study of its fracture toughness and failure analysis is gaining more relevance [2]. This is done through fracture mechanics. Fracture mechanics is the study that relates applied stress, flaw size and the material's fracture toughness to determine whether or not these conditions lead to failure, which is indicated by an unstable growth of the flaw, or crack. In figure 1 a comparison between the fracture mechanics approach to analyzing a design and the traditional method is shown. As it can be seen, the traditional method only takes into account the applied stress and the material's strength, which is too simplistic to study the crack behavior.

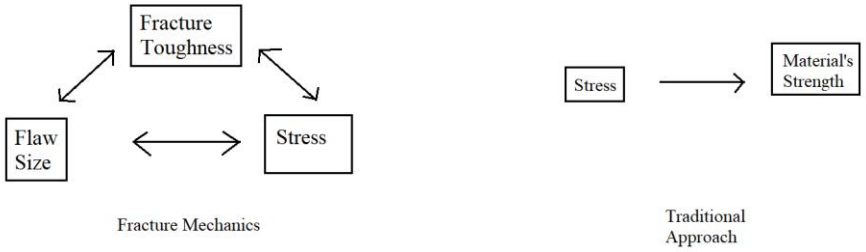

Figure 1: Comparison between the fracture mechanics approach and the traditional approach.

The polymer used in this study is the Poly(vinylidene fluoride), or PVDF. It was created and commercialized by DuPont in 1948 and 1961, respectively. It is used in the industry because of the high temperature it can withstand, 130°C,as well because of its high mechanical properties. It also possesses other interesting properties, such as high chemical resistance, it is nontoxic and it can be processed using several industry standard processes, such as extrusion, injection molding, thermoforming and blow molding [3].

One of the applications is in the oil and gas industry. As the offshore oil industry is continuously progressing into deeper waters, so is the need for developing materials able to withstand the new and harsher working conditions. In deeper waters, the materials have to be able to withstand loads under greater pressure, more extreme temperatures and in contact with more aggressive fluids.

In this application, the PVDF is used in the flexible riser. These are pipes that transport the fluid from the subsea facilities to the topside facilities. They are made of several layers that can be made of metallic alloys and polymer. These layers are divided into: Carcass, Inner Sheath, Pressure Armor, Anti-wear layer, Tensile armor, Polymer layers and Outer sheath. Out of these, the Inner sheath, Outer sheath, Anti-wear layer and Insulation layer are made of polymeric material. More specifically, the Inner sheath and Anti-wear layer can be made of PVDF, due to its chemical resistance and thermal stability [4]. In Figure 2 a

schematic image of a flexible riser is show, and the components that can be made of PVDF are indicated.

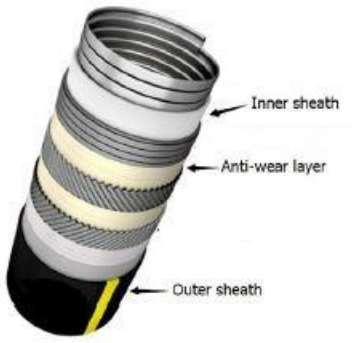

Figure 2: Flexible riser, adapted from [4].

To study the material's response to the mechanical load applied in this application, mechanical tests should be done in an aggressive environment, in order to mimic the working conditions as much as possible and obtain the most accurate data possible. However, this leads to many practical problems, such as possible damage to measuring devices, since they would be in the aggressive environment as well.

In this work, a non-standardized method, the S_{Pb} method, which is based on the load separation principle, is used, with the aid of a digital image correlation study, to analyze and compare the fracture properties of two commercial grades of PVDF. The method is based on the ratio between the loads of two separated specimen, which makes it attractive since the instrumentation to measure only load is much simpler than the one needed to measure strain or displacement. The Digital Image Correlation is a method to study the deformation fields through a series of images taken during the test, allowing for an extensive study and, more importantly, being free of any direct contact with the specimens, which is particularly useful when there is an interest in testing under aggressive environments.

The objective of this study is to determine whether the S_{Pb} method can be applied to this polymer, as well as if the results it yields are accurate.

2. State-of-the-art

2.1. Polymers

A polymer is a material composed of a great number of repeating units, which can reach millions. This kind of material is composed mostly of carbon. These units are linked by covalent bonds [5].

Since there are many existing repeating units and several ways of combining them, there is a huge number of polymers with different physical and chemical properties, which make them very versatile and able to be used in many different applications. This can be seen in the different uses polymers have today. For example, they can be used as simple plastic toys or as intricate materials in the bioengineering industry or as coating against corrosion used in the oil and gas industry. Some examples can be seen in figure 3.

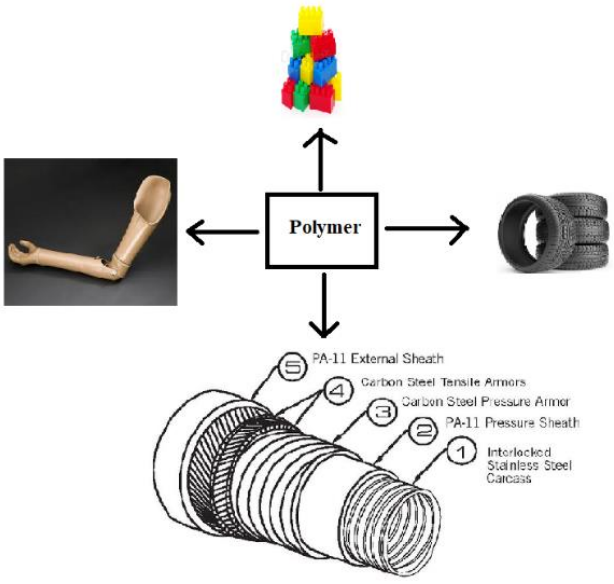

Figure 3: Some of the modern polymer application.

Polymers can be classified in thermoplastics, thermosetting and elastomers.

2.1.1. Thermoplastics

Thermoplastics are polymers that can be molded in a lot of different shapes using different processing techniques, such as extrusion. They can be reprocessed any number of times, as long as there isn't extensive damage or contamination in its chains. This is possible due to the fact that the polymeric chains interact through the weak intermolecular forces. Since they are weaker than the covalent bonds which constitute de chain, they break first when heat is applied and this allows the chain to move and, therefore, the material can be molded. This means that polymeric chain is formed by strong covalent bonds, while the forces between them are weak intermolecular forces. This makes the thermoplastics also display highly anisotropic behavior.

This type of polymer can be either amorphous or semi-crystalline, which means they can present both a crystalline phase and an amorphous one. The crystalline phase has a unique temperature, the melting temperature. This is the temperature at which the crystalline phase melts and the material is completely amorphous. The amorphous phase, on the other hand, has as characteristic temperature the glass transition temperature. At this temperature the material goes from the glassy state to a rubbery state [1].

The thermoplastics constitute, by far, the most used polymer in the industry [1]. Some examples of thermoplastics are: Polyethylene, Polyvinylidene fluoride, polyamides, etc.

2.1.2. PVDF

Polyvinylidene Fluoride is a semi-crystalline thermoplastic. Its repeating unit is shown in figure 4. The bond between carbon and fluorine is strong and, therefore, hard to break. This gives the PVDF a high chemical resistance as well as thermal stability. Due to the position of the fluorine atoms in the repeating unit, there isn't polarization in the polymeric chain and they are not under great repulsive forces. This allows the chains to arrange

themselves in a more compact way, which can lead to a high crystallinity, depending on the thermomechanical process used. The crystallinity is usually between 32 % and 76 % [3].

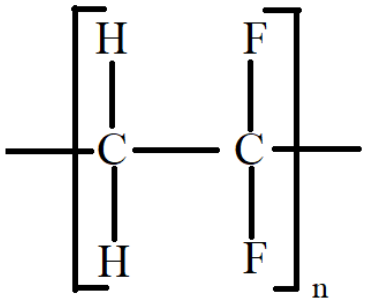

Figure 4: Polyvinylidene Fluoride's repeating unit.

Its glass transition temperature is between -57 °C and -29 °C and its melting temperature is between 158 °C and 200 °C. These ranges can change depending on additives and chain size. Due to its strong bonds between carbon and fluorine, this material can be used at temperatures up to 130 °C. It also displays a greater mechanical strength when compared to other thermoplastics and it can also withstand a greater number of loading cycles [3].

The high working temperature at which it can be used, as well as its mechanical properties and chemical resistance, make the material very attractive to a lot of different areas. It is mostly used in applications that present harsh conditions, such as presence of chemical products, high temperature or pressure.

Nowadays, PVDF is also being used in the oil and gas industry as a pressure barrier in risers. Before this, the polymers used were polyethylene and polyamide. However, as the environments got harsher, the materials used in this sector needed to be adapted, and PVDF became a viable option.

Processing this material is a little bit difficult due to its composition and intermolecular force, so there were created several commercial grades, which may contain plasticizers to ease the process [6].

2.1.3. Mechanical Properties

One striking difference between polymers and other materials is the way they behave when under mechanical solicitation, either strain or stress. While metals and ceramics are independent of loading rate, the polymers' mechanical behavior is heavily time and temperature dependent. At lower temperatures and higher loading rates, they present an elastic behavior, very similar to metals and ceramics, while at high temperatures and low loading rates, they present a viscous one, flowing like a viscous fluid. Therefore, they are usually referred to as viscoelastic [1]. In figure 5, an example of how the test rate can affect a viscoelastic material's response is given.

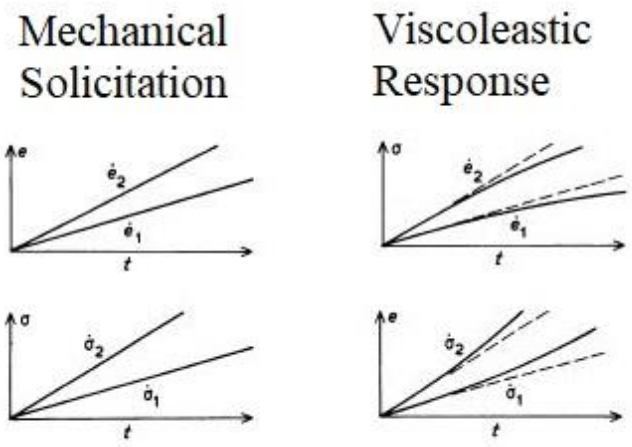

Figure 5: Viscoelastic behavior, adapted from [1].

To predict the mechanical behavior of this material, models were created. They usually assume that the deformation of a polymer can be divided into two components: an elastic and a viscous component. Each component follows a different law. The simplest models consider that the elastic deformation follows only Hooke's law and the viscous

deformation follows only Newton's law. So, each component is represented in the models as a mechanical component. The elastic one is represented by an elastic spring, while the viscous is represented by a viscous dashpot. Based on these considerations, several models were created, arranging these elements in different ways [1].

A polymer's response to loads is heavily dependent on the temperature, not only due to the viscoelasticity, but also because of the transitions, namely melting and glass transition. It is important to note that these transitions happen over a range of temperature, not on a single temperature. The glass transition temperature and melting temperature are usually defined as the average temperature in the range [7].

When a polymer is below the glass transition temperature, its chains don't have enough energy to allow slipping, which means they don't have mobility and can't change their conformation. When this is the case, the polymer is in a glassy state, which is characterized for being hard and brittle [1].

On the other hand, when a polymer is over the melting temperature, its crystalline phase melts and disappears. This happens because there is enough energy to break the intermolecular bonds between the chains in the crystalline phase, which changes the material from a rubbery state to a viscous state. Since this transition only affects the crystalline phase, it only takes place in the semi-crystalline polymers [5]. In the figure 6, there is a curve presenting the usual behavior of a polymer's Young's Modulus with increasing temperature of an amorphous polymer and a semi-crystalline one.

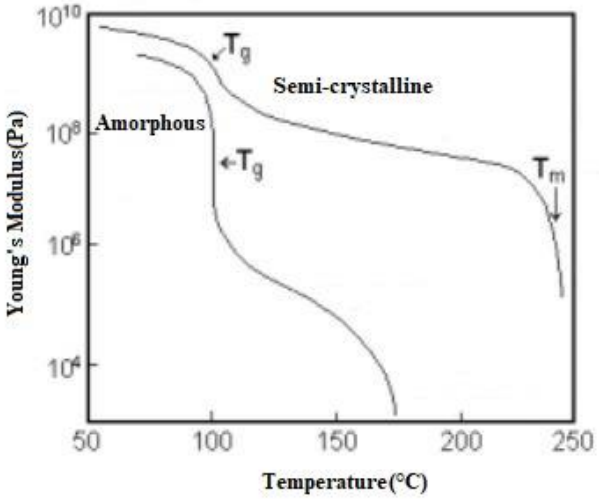

Figure 6: A polymer's Young Modulus behavior with increasing temperature, adapted from [8].

2.1.4. Deformation Mechanisms

As mentioned before, thermoplastic polymers may consist of both crystalline and amorphous phases. Each one has different deformation mechanisms. The crystalline phase has mechanisms similar to other crystalline materials, such as metals and ceramics, while the amorphous phase has completely different ones.

The crystalline phase's deformation mechanism are: slip, twinning and phase transformations. Out of these three, slip is the most important, because it is the one that produces the largest plastic strain [9].

As it is the case with metals, a slip system, a combination of a slip direction and a slip plane, is needed in order to have the slipping occur. For the material to present significant plastic strain through this mechanism, 5 independent slip systems are necessary. This is not usually the case with polymers due to their crystalline structure, which lacks the symmetry observed in metallic materials. Usually, when this type of deformation happens, the main mechanism is the chain direction slip, which involves a movement of the molecules in relation to each other parallel to the chain direction. Even though this mechanism is the

crystalline phase's main deformation mechanism, as it was said before, it doesn't allow for great plastic deformation, due to the small number of independent slip systems. However, most polymeric materials display a significant amount of plastic deformation. This means that probably most of the plastic deformation is due to the deformation mechanisms in the amorphous phase [9].

Similar to metals, the crystalline phase in polymers consists of unit cells. However, unlike metals, polymers' atoms are not in a simple close-packed array. This is because in the case of metals, the unit cells contains only a few atoms, which allows for a simple cubic or hexagonal geometry, while in the case of polymers, the unit cells consist of repeating segments of the polymer chains packed together. This means there can be hundreds of atoms in the unit cell. This complexity leads to unit cells having complex geometry, such as orthorhombic, monoclinic or triclinic, which don't display as much symmetry as the cubic unit cells. This leads to fewer slip systems and, therefore, to a smaller deformation due to slipping [1]. For example, in the case of the PVDF, its unit cells can be either monoclinic or orthorhombic [3]. In figure 7, there is a schematic image showing an example of a polymeric unit cell.

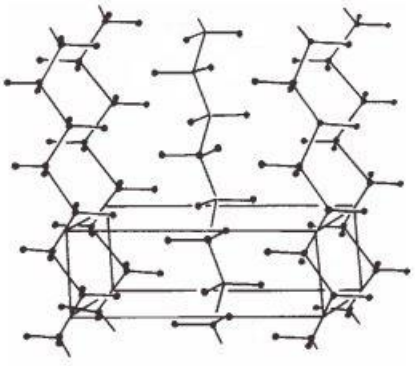

Figure 7: Schematic image of a polymer's unit cell, adapted from [7].

Other mechanisms also exist, such as the interfibrillar slip and the transverse slip, but they are not as pronounced as the chain slip. Twinning may also happen in the crystalline

phase if its structure is asymmetrical enough. The behavior and phenomenon are the same as in the metals. The 2 basic twinning modes are {3 1 0} and {1 1 0}. At last, martensitic transformation may also happen due to the application of stress to the crystalline phase [9].

Besides the crystalline phase's deformation, there is also the deformation that takes place in the amorphous region. This region is between the crystals in the structure and hold them together. The deformation of the amorphous phase happens through interlamellar slip, interlamellar separation and stack rotation [7].

The interlamellar slip consists of the shearing of crystals parallel to each other while the amorphous phase undergoes a simple shear deformation. HDPE was studied and it was determined that elastic deformation happens mostly through reversible interlamellar slip. This reversibility is due to the fact that during the elastic deformation, the tie molecules between crystals are extended and, when the stress is removed, they tend to pull the crystals to their original position [9].

When a stress is applied in the direction parallel to the lamellae's surface, interlamellar separation can occur.

Stack rotation can only happen if the lamellae are in the shape of a stack, which is free to rotate when under stress, and if the stack is surrounded by amorphous material that can absorb all the distortion caused by the deformation.

The different deformation mechanisms in the amorphous make up for the fact that the crystals lack symmetry and, therefore, don't meet the requirement to present a large plastic deformation through slip [9].

At last, we also have deformation mechanisms related to the spherulites. They consist of crystals that grew radially from a nucleus and are linked by a constricted amorphous phase between each crystal [1]. When a mechanical solicitation is applied to the material, these structures also deform according to some mechanisms. The mechanism a spherulite displays when responding to mechanical solicitation may vary depending on its

size. Large spherulites may display crazing and cavitation, which can lead to a brittle behavior, while small ones display homogeneous fragmentation, which can lead to a larger amount of plastic deformation. Both of these process are continuous through the boundaries between two spherulites, which leads to stress transfer from one spherulite to another. The deformation of the spherulites can be seen using AFM. With this technique, it was observed that plastic deformation leads to the stretching of the spherulites in the same direction as the mechanical solicitation is applied. Also, it was determined that the plastic deformation leads to different spatial arrangement of the regions of the spherulite [10].

2.2. Digital Image Correlation

Digital Image Correlation is a method that consists of comparing images of the same scene, usually an object under stress, and creating the displacement or strain field that best describes it. The comparison between the images can be very accurate and pixel-sized features can be shown. This method is interesting in mechanical testing for several different reasons: Image acquisition does not require contact with the specimen, which makes it viable for a large number of environments; more advanced digital cameras can provide images with a high frequency, which allows for dynamic tests; the use of more than one camera allows the creating of full three dimensional displacement and strain fields; this analysis usually contains data of a larger region of the material in comparison to the classic instrumentation, such as extensometers [11].

This technique is of particular interest when analyzing the discontinuities created by the presence and growth of cracks. Because of the nature of the analysis, it can be used in small specimen, as well in large structures [11].

One of the basic principles of the DIC is that the image is only deformed by the in-place displacement field, without any changes on the gray levels. So, the deformed and reference images can be related by the Equation 1:

$$G(x) = f(x + u(x)) \quad (1)$$

However, changes in the lighting of the object may happen due to the deformation. These changes also lead to modifications to the gray levels. This means that the equation has to be adapted to Equation 2:

$$G(x) = \big(1 + a(x)\big) f\big(x + u(x)\big) + b(x) \quad (2)$$

Where b is an offset and a is a rescaling factor.

At last, there is always noise in the image acquisition, even if it is a small amount. Therefore, to make the algorithm more robust, another factor is added, leading to Equation 3:

$$G(x) = f\big(x + u(x)\big) + n(x) \quad (3)$$

Where n is the noise amplitude.

Determining the u(x) is a problem when dealing with DIC algorithm, especially if the conservation of the gray levels are relaxed by considering other factors, such as the lighting and the noise. To make the calculation possible, other constraints, called regularizations, are added. They consist of restricting the variability of the displacement field. This is usually done by assuming that u(x) is either piecewise constant or varies linearly with x, allowing for arbitrary discontinuities. Another regularization can be to assume a global continuity for u through decomposition over finite element shape functions. In the case of crack analysis, the regularization is done through a priori knowledge of analytical displacement fields [12].

2.3. Fracture mechanics

The study of fracture mechanics can be divided into different categories, based on the material's behavior when stress is applied to it. The main categories are: linear elastic fracture mechanics, elastic-plastic fracture mechanics, viscoelastic fracture mechanics and viscoplastic fracture mechanics.

The linear elastic fracture mechanics is applied to materials that follow Hooke's law until they fracture, with no or small amount of plastic deformation confined to a small region on the crack tip. Or, in other words, it can be used to materials that present linear and elastic behavior until they fracture. This theory consists of using the Griffith Equation as well as the stress intensity factor K. Due to its restrictions, this theory can only be applied to brittle materials, such as ceramics, polymers bellow the glass transition temperature and high strength steels [2].

The elastic-plastic fracture mechanics can be applied to materials that present plastic deformation or, in other words, that don't present only a linear and elastic behavior, and that are time-independent. When this theory is applied, two methods are usually used: crack tip opening displacement, or CTOD, and J integral. Due to its much less restrictive nature, this theory can be applied to most metallic alloys [2]. The J integral is a path-independent line integral which has a value equal to the decrease of the potential energy per crack size and can be used in linear and non-linear elastic materials. Since it is path independent, the J integral can be considered as a measure of the intensity of the stresses at the tip of notches and cracks. Therefore, there is a parameter J_{IC} that defines the onset of the crack propagation [13].

In the case of viscoelastic materials, some methods used for time-independent materials are adapted, such as the J integral. To be applied to a range of viscoelastic materials, the J integral was generalized by Schapery. This adaptation used the nonlinear viscoelastic constitutive equations, as well as the correspondence principle, which related the stress and strain between two bodied, one elastic and the other viscoelastic. The other factor that had to be considered when dealing with polymeric materials is the transition from linear to nonlinear behavior, which happens from low to high stresses. To address this issue, Schapery used a modified constitutive equation, where the strain consists of the sum of two integrals: one related to the linear portion and another related to the nonlinear one [13].

There are different methods to determine J integral. One of them is the S_{Pb} factor method. This factor is the ratio between the loads of a pre-cracked specimen and a blunt notched specimen, both with the same geometry, when a fracture test is performed. This method is based on the load separation property, which not all materials present. When a material presents this principle, its load can be considered as a product of two independent functions: a geometry function and a material deformation function. So, the load can be written as it can be seen in Equation 4 [14].

$$P = G(\frac{a}{W}) \times H(\frac{v_{pl}}{W}) \quad (4)$$

Where P is the load, G is the geometry function and H is the material deformation function.

The S_{Pb}, then, can be defined with Equation 5:

$$S_{Pb} = \frac{P_p}{P_b} = \frac{G(\frac{a_p}{W}) \times H(\frac{v_{pl}}{W})}{G(\frac{a_b}{W}) \times H(\frac{v_{pl}}{W})} \quad (5)$$

Where a is the crack length value, W is the width of the specimen, v_{pl} is the plastic displacement. Also, the subscript P indicates the function is related to the pre-cracked specimen, while the subscript b indicates the function is related to the blunt notched specimen.

Since this method compares two specimens of the same material, their H function is the same and we, then, Equation 6:

$$S_{Pb} = \frac{P_p}{P_b} = \frac{G_p}{G_b} \quad (6)$$

In other words, the S_{Pb} factor depends only on the geometry and any change in its value is due to changes in the geometry of the specimens, which includes the crack size. Due to the nature of the fracture test, the shape of both specimen don't undergo any change during the test, since all the stress is located in the crack tip. Also, due to the larger crack tip radius, the blunt notched specimen is going to present crack propagation at later moments compared to the pre-cracked one. This results in the consideration that any

changes in the S_{Pb} factor is due to change in the geometry, more specifically to crack growth in the pre-cracked specimen [15].

This method is attractive because the only measurements it requires are of load and displacement. Both of these are of relative easy to measure, when compared to the other measures needed in other fracture mechanics methods, such as CTOD. This makes it interesting to apply when an aggressive environment is considered, since the instrumentation used to measure both load and displacement don't need to be in direct contact and, therefore, are not affected by it.

3. Materials and Methods

3.1 Specimens

The tests were made with 2 commercial PVDF, PVDF A, and PVDF B. The PVDF A had about 3 % to 5 % of plasticizer, while PVDF B is a copolymer with polyethylene in it. They were extruded and machined for tensile tests and 3 point bending tests. The tensile tests focused on typical stress-strain behavior, while the objective of bending tests was to characterize the fracture behavior of each material and, also, the sample size effect associated the fracture mechanics methodology.

The tensile tests samples were machined following ASTM D638-14 standard; and the geometry is illustrated in figure 8. The three point bending tests geometries used here can be seen in figure 9, and their dimensions are: 40.5 X 9.2 X 4.6 mm (small), 60.7 X 13.8 X 4.6 mm (medium) and 80.1 X 18.4 X 4.6 mm (large). These dimensions were chosen to keep the thickness constant and keep the ration between the length and width constant. The small one was the first one to have its geometry defined and it followed the ASTM D-606896 standard, and the medium and large specimen had its dimensions as 1.5 and 2 times the length and width of the small specimen. In figure 9 the machined specimen can be seen. For each geometry size, the samples were either pre-cracked or blunted notched. The pre-

crack and the blunt notch reached a/W=40 % and a/W=50 % of the sample' thickness. The pre-crack was opened first with a circular saw and, then, sharpened with a blade. The blade is used to cut through the last 3 mm in every geometry. The blunt notched was made with a 2 mm diameter drill and it was made in such a way that the distance between the tip of the blunt notch and the end of the cut made with the saw is 3 mm, in other words, the same size as the pre-crack made with a blade. In the blunt notched case, the hole was drilled first, then an opening was made with the circular saw and, at last, the razor blade was used to connect the cut made by the circular saw and the hole. This order was used to guarantee that the razor blade would not cut through the hole and reach the other side. If this were to happen, a defect would be created as a result and it would concentrate stress and it would grow as a crack. A schematic image of the samples with the holes' and cuts' dimensions can be seen in figure 10. In Figure 11 there are two blunt notched and one pre-cracked specimen made of aged PVDF A.

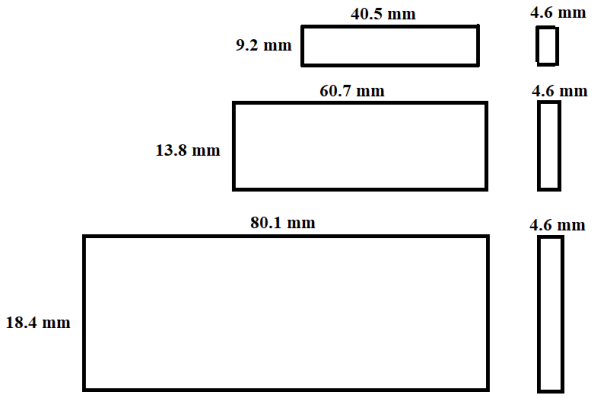

Figure 8: Fracture test specimen dimensions: small, medium and large, from top to bottom.

Figure 9: Fracture test specimen without pre-cracks or blunt notches.

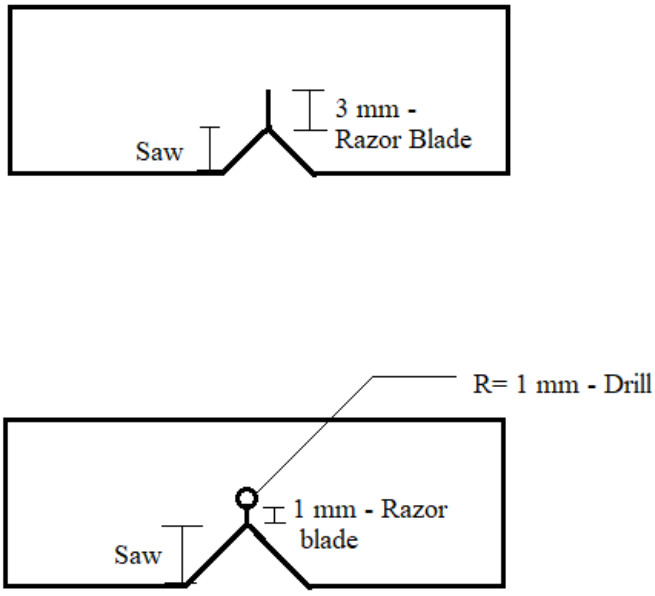

Figure 10: Relation between the pre-crack and the blunt notch.

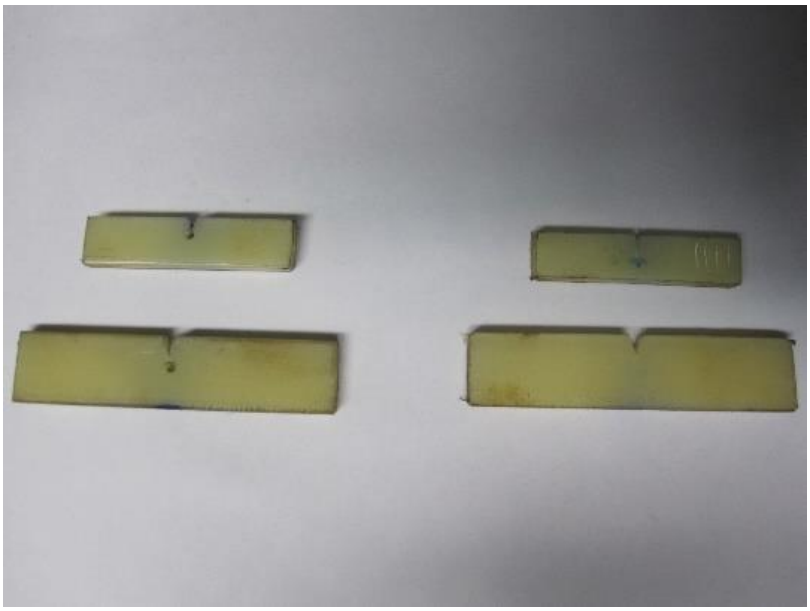

Figure 11: Aged blunt notched and pre-cracked specimen

PVDF A was also annealed in order to compare the effects of thermal aging on the material's mechanical behavior. It was aged in an oven for 21 days at 120 °C. The material before and after the aging can be seen in figure 12 .After aging, it was also machined into tensile test samples as ASTM D638-14 and into three-point bending specimen, using the same dimensions as before.

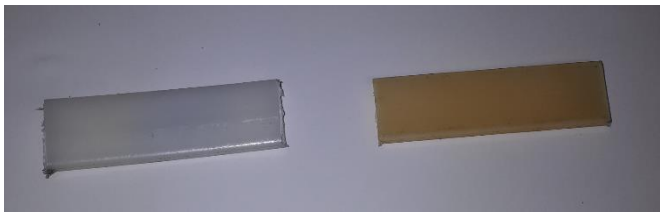

Figure 12: PVDF A before (left) and after annealing (right).

3.2. Mechanical Tests

The mechanical tests conducted, tensile and fracture toughness tests, were both at room temperature. The tensile test was performed with 50 mm/min crosshead speed. The fracture test was done at two crosshead speed, regardless of the geometry: 10 mm/min and 100 mm/min. The crosshead speed used during the tensile test was chosen only with the

material's characterization in mind, while the crosshead speeds chosen for the fracture tests were used to evaluate the test rate effect on the material's properties. If the calculations to determine the J integral were to be done, the crosshead speed chosen in this test would have to be the same as the one used in the fracture test. In total, 3 tensile tests were done on different PVDF A specimens. The PVDF B was not subjected to this test because of the restricted amount of material that was available. Both of these types of tests were done with the Universal Testing Machine INSTRON 5567. The machine control and data acquisition was accomplished through BlueHill 3 software. The tensile test is pretty much standard, while the fracture toughness is based on load and crosshead displacement measurements. The data analysis was processed in Microsoft Excel and Origin Pro 8, whenever suitable.

The tensile test, per ASTM D-63814, determined the Young's modulus and the yield point, and the deformation at rupture was measured. The fracture toughness tests followed the standard ASTM D-606896, which determines the roll size, as well as the specimen geometry. It is worth mention that, per D-606896 standard, only the medium sized sample used here is specified. Nonetheless, two other geometry were employed to evaluate the effect of the geometry on the crack initiation and propagation.

The fracture toughness test was done by supporting the sample in static steel rolls, which have 10 mm radius, whilst span depends on the length of each sample geometry, and the load is applied through a steel roll on the opposite face to the pre-crack or blunt notched. This typical arrangement allows a tensile stress field at the crack tip. Ideally, fracture toughness tests require that all strain field must be directed to crack tip, where the process zone takes place; however, it does not happen in many cases, and the common reason is attributed to the steel rollers that causes indentation on the soft sample under it. To correct the indentation effect, the standards themselves recommend to test the same geometry and size, without any notch or pre-cracks, and to measure the load-displacement curve, which will be then subtracted from the result originated in testing notch or pre-cracks samples. This

approach allows to analyze only the load applied at the crack tip. The test setup can be seen in figure 13.

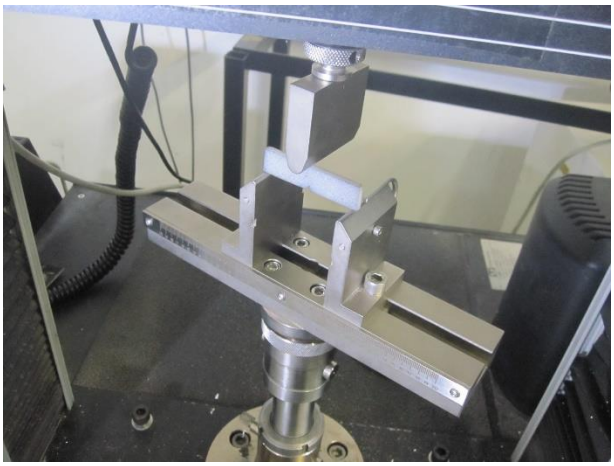

Figure 13: Fracture test setup.

Even following the ASTM D-606896 and good laboratory practices, some of the largest specimens were pushed off (ejected) from the test setup, probably due to the fact that they were not made perfectly straight (or parallel) during the machining and the geometry led to loads in the outward direction – these were lost samples. This problem was corrected, however not all conditions were analyzed because of the restricted number of specimens.

3.3. Digital Image Correlation

Besides the load and crosshead data analysis, the Digital Image Correlation (DIC) technique was used to study strain field at the crack front. Briefly, it is an optic-based technique used to determine 2D or 3D field maps on a material's surface while it is being mechanically loaded. Through them, it is possible to determine displacement, deformation, test speed, curvature, etc. The strain field determination is done by comparing several digital images taken in different deformation stages (time). The software, then, tracks the movement of pixel blocks to create a displacement map and a strain map. Since DIC

techniques don’t require direct contact with the sample and it is independent of the material and length scale, it can be used in several applications.

To obtain the DIC data and conduct its analysis, the samples were painted with black spray paint. This is done in order to leave black dots on the surface to create color contrast. This contrast allows the software to measure the dots’ displacement more accurately. Usually, a white paint is also applied in a continuous manner before the black dots are made, to increase the contrast even more. However, in this case, the white paint could not be applied because it formed a film over the crack region, impairing the local data acquisition/analyzed. Other than that, to ensure there would be no problem tracking the points during the image processing stage, a good lighting setup was used during the test, to make it every region in the image clearly visible with no shadows, the camera focus was adjusted to capture the most details in the specimens and the image was processed with different filters after the test. During the test with the 10 mm/min rate, the camera stored imaged at a rate of 5 images per second, while during the tests with 100 mm/min rate, the capture rate was 14.8 images per second, which is the upper limit of the camera. In figure 14 the painted specimen can be seen and in figure 15, the test setup with the camera is shown. While the tests done with crosshead speed of 10 mm/min have a satisfying amount of images taken, it is believed that the ones done with crosshead speed of 100 mm/min did not. However, 14.8 was the limit imposed by the hardware used.

Figure 14: Fracture specimen painted for DIC analysis.

After the images were taken, they were treated with the software Image J. Image J is an open source software developed by the National Institutes of Health used to process images, which means it can control the contrast and brightness in the image, as well as apply different filters, such as binary filters, to the image. In this software, the contrast was enhanced before applying a binary filter. This is done to make the material completely white and the dots completely black. This process was applied to all images to make the contrast and pixel tracking faster and more precise. After this, it was applied a watershed filter. This filter distinguishes 2 particles, in this case black dots that overlap. At last, the image was despeckled in order to reduce the noise. Also, since color is not a factor that influences the analysis, the image was converted from 16-bit to 8-bit to make the images lighter and easier to handle. In figure 16 the Image J's interface can be seen. In figure 17, an example of an image after all the treatment is shown.

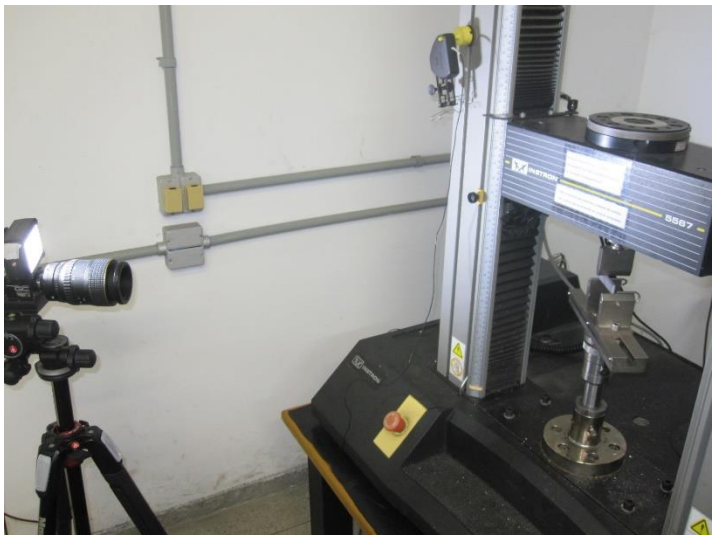

Figure 15: Fracture test setup with DIC camera.

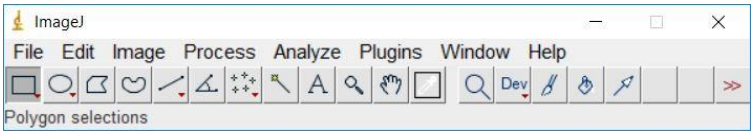

Figure 16: ImageJ software

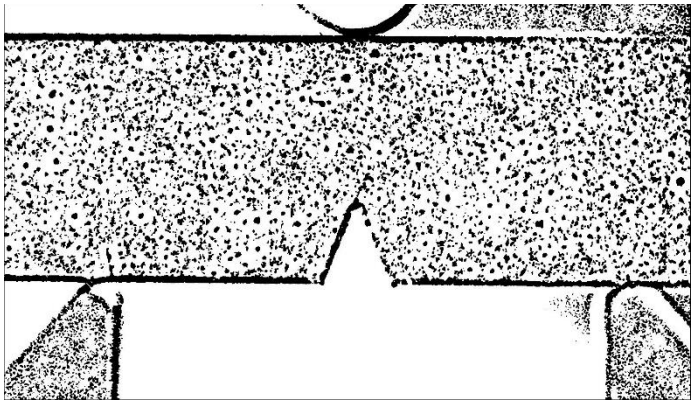

Figure 17: Example of large specimen image after being processed with ImageJ.

After the process, the images were analyzed in the software nCorr. It is an open-source software that runs on Matlab and is recommended by the international Digital Image Correlation Society. This software is used to analyze a series of images and create a displacement and a strain field, based on the Digital Image Correlation principles. In figure 18 nCorr's interface can be seen. This software was chosen because it is was the only one among the ones recommended by the International Digital Image Correlation Society that

was able to handle the crack propagation on a polymeric material. Before using this software, the following programs were also tested: Ecorr, Yet Another Digital Image Correlation Software and Digital Image Correlation Engine. The latter two are also recommended by the International Digital Image Correlation Society. However, even using this software, it was not possible to study the crack propagation until the end of the test. This is probably due to the fact that these softwares were made to analyze smaller amounts of deformation, such as in the case of metals, and their algorithm cannot process the larger amount of deformation in the tests performed. This leads to slow iterations and most of the time the analysis would not converge to a solution. In the rare occasions it converged, the mesh created ended very distorted and deformed, making it not fit for any analysis.

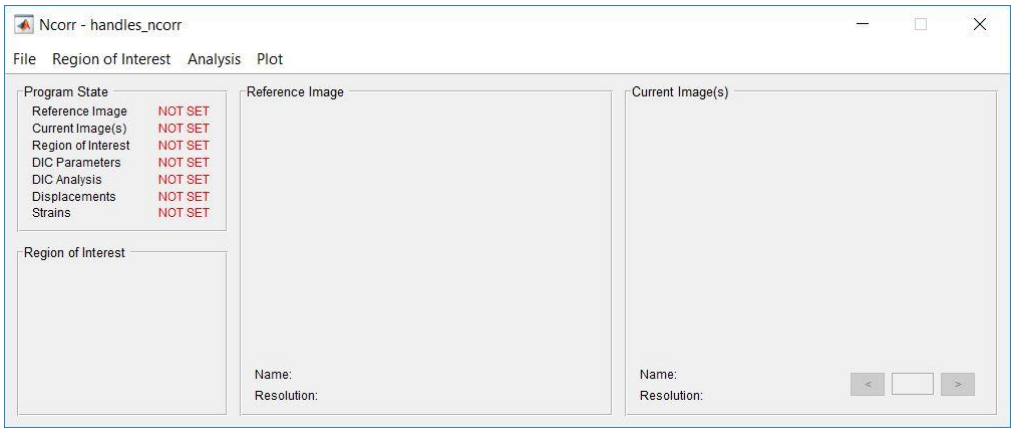

Figure 18: nCorr software interface.

The interest in this analysis was determining the moment the crack starts growing, consequently, not all images were analyzed. This was done to save time, since analyzing more images would take much more time, to make the current analysis in reasonable time frame and to make the analysis possible, since when a great amount of deformation is present, the software cannot finish the process. For instance, when every individual image taken in a test was used, the software was not able to complete the analysis, possibly due to the fact that the displacements were much greater than the algorithm could compute since polymeric materials present high ductility.

DIC is a surface measurement technique and, inherently, it only allows a plain stress interpretation. The middle thickness, sometimes, may be in plain strain, and crack growth could happen. In order to verify whether a crack has grown through the thickness during the test, dye penetrant was applied after the fracture toughness specimens were tested. The dye penetrant stayed for 15 min on the specimen, the excess was removed and allowed to dry for 2 hours. Subsequently, the specimens were immersed in liquid nitrogen for 20 minutes, in order to reach the complete brittle state (well below its T_g), and then broken. Under this procedure, any crack propagation that happened during the test was not affected by the breaking process, because the dye penetrant allows to see whether a crack length occurred after the crack growth caused by the test, regardless of the propagation mode. Then, both halves of the specimen were taken to the microscope, where the fracture surface was analyzed. In the microscope, images were taken with 8x and 10x magnification. Due to some features observed in the microscope and its limited magnification, other samples of tested specimen were, again, broken in a brittle state and taken to a Scanning Electron Microscope. The microscope used could not hold samples with heights greater than 5 mm. To adapt the samples to this condition, the specimens were sawed 5 mm from the fracture surface. Other than this geometrical adaptation, no other sample preparation procedure was adopted, however during the analysis, each sample only remained in the equipment for a short time, as to not degrade the surface. In this analysis, the magnification varied from 50x up to 250x. Both microscopic analysis were done to both materials and to specimen tested with a crosshead speed of 10 mm/min and 100 mm/min. However, only pre-cracked specimen were analyzed since the blunt notched ones don't present considerable crack growth.

One major problem that was not solved during this work was the difficulty to use the DIC to analyze the displacement maps when blunt notched specimens were tested. When this type of specimen was studied, the software was not able to reach a solution and create

a displacement map. This is probably due to the increased complexity created by the introduction of the hole in the middle of the specimen. This factor added to the larger deformations may not have been foreseen by the software developers and the analysis was not completed. In these cases, the program took an abnormally long time to process each frame and in the end, an error regarding the mesh would occur.

3.4. Differential Scanning Calorimetry

Mechanical properties do materials are very dependent on their structure and, regarding polymers, the volume fraction of crystalline phase has been quite determinant. Differential Scanning Calorimetry (DSC) is a technique often used in the polymer area to analyze thermal transitions, such as melting and crystallization. The samples testes here went through only one cycle because the main interest was to compare the properties between the as-processed and thermal aged one – the thermal aging was conducted at 120 ºC for 21 days.

The melting point can be identified as an endothermic peak since it is a first-order thermal transition. In polymeric materials, the crystals don't melt at once, at the same temperature, they melt in a temperature range. But, the melting temperature is defined as the temperature of the highest point in the peak. With the endothermic peak, it is possible to determine the material's crystallinity, in other words, the fraction of material in the crystalline phase. To do so, a baseline is created and, based on it, the peak area is calculated. With the calculated area, we have the relation given in Equation 7:

$$\int heat\ flow\ dt = [J.\frac{K}{g}.s] \quad (7)$$

Dividing this value by the heating rate we have, then, Equation 8:

$$[J.\frac{K}{g}.s.\frac{s}{K}] = [J/g] = \Delta H_m \quad (8)$$

ΔH_m is the material's melting enthalpy. To calculate the crystallinity, we divide this value by the hypothetical melting enthalpy of the 100% crystalline material, which is 104.5 $J.g^{-1}$.This means that the crystallinity can be determined by Equation 9 [3]:

$$X_C = \frac{\Delta H_m}{\Delta H_m^{100}} \quad (9)$$

This thermal analysis was done in the PVDF A, both as-processed and aged. The equipment used is shown in figure 19. The method is based on heat flow, and the cycle used was heating from 25 °C to 220 °C with a heating rate of 10 K/min, maintaining the temperature for 10 minutes, and cooling from 220 °C to 25 °C, with a cooling rate of 10 K/min. The whole test took 49 minutes (1 run). The samples were taken from the bulk and weighted around 10 mg. The tests were done in a nitrogen atmosphere to avoid any reaction between the material and the atmosphere. The crucible used is made of an aluminum alloy and weights 10.39 mg, with the top pierced. Also, nitrogen was also used as protective gas and to purge. The purge flow was 20 ml/min and the protective flow was 50 ml/min.

Figure 19: DSC equipment.

The results were analyzed by the software NETZSCH Proteus.

4. Experimental Results and Discussion

4.1 Specimen Characterization

In Figure 20, a typical the stress-strain curve made from the tensile tests (done with the annealed PVDF A) can be seen. Based on this curves and the data from the tests, the Young modulus, yield point and rupture stress were determined.

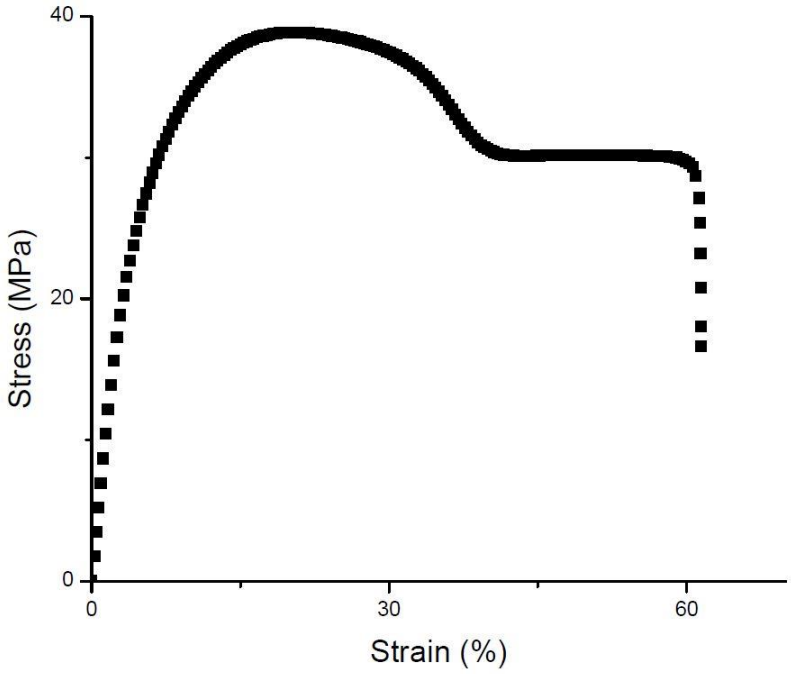

Figure 20: Typical stress-strain curve of the aged PVDF A.

In the figure 21 there are the curves from the DSC tests done on the annealed and unaged PVDF A. Based on the peaks area, in other words, based on the melting enthalpy, both material's crystallinity were calculated. The peak area was determined based on a baseline, which was defined by the point where the DSC curve deviated from linearity. The same baseline was used for both materials, to make the comparison possible. The annealed material has a crystallinity 7.4 % greater than the unaged one. An increase in crystallinity was expected because the temperature at which the material was annealed was high enough to promote crystallization. So, since this process lasted for 21 days, there was enough time for the more crystalline phase to form.

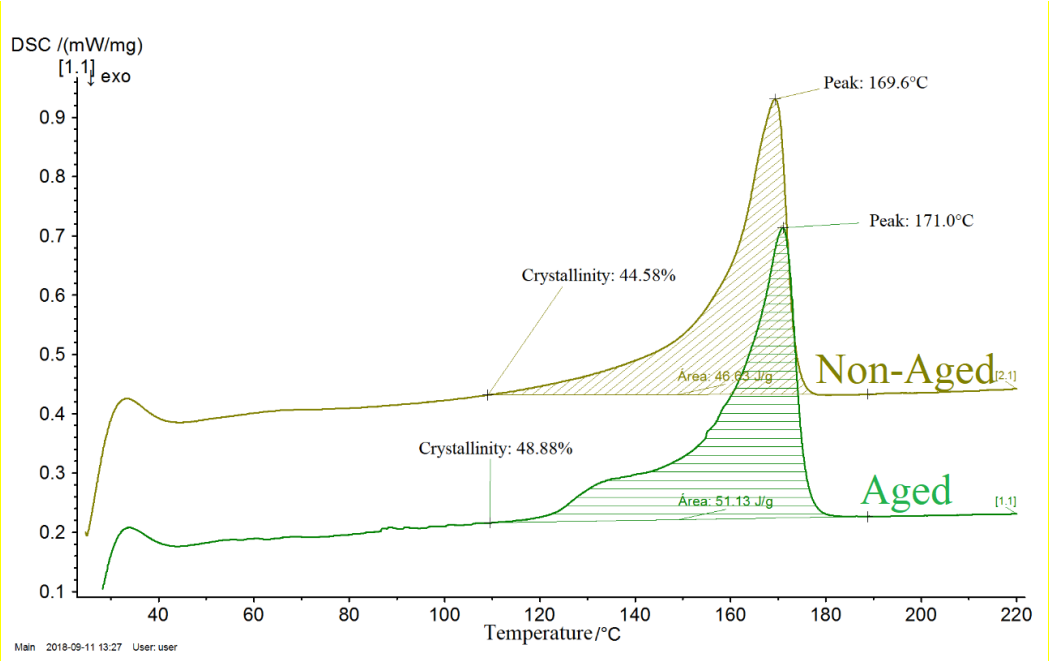

Figure 21: DSC comparison between aged and unaged PVDF A.

4.2 Fracture Tests and DIC

In the figure 22, there are the typical load-displacement curves of the largest samples. They can be pre-cracked or blunt notched at different depths and were tested at different rates. The same curves for large specimen with other crack depth and crosshead speed are in the annex and follow the same tendency, but with slightly different load levels. In figure 23, there is the same kind of curves, but for the medium-sized samples and in figure 24, we have the curves for the smallest samples. All of them were tested with a crosshead speed of 10 mm/min and had a crack depth of a/W=50 %. The same type of curves were made using the data from the tests of PVDF B. They displayed the same tendencies as the ones made using PVDF A, but with slightly different loads. They can be seen in the annex.

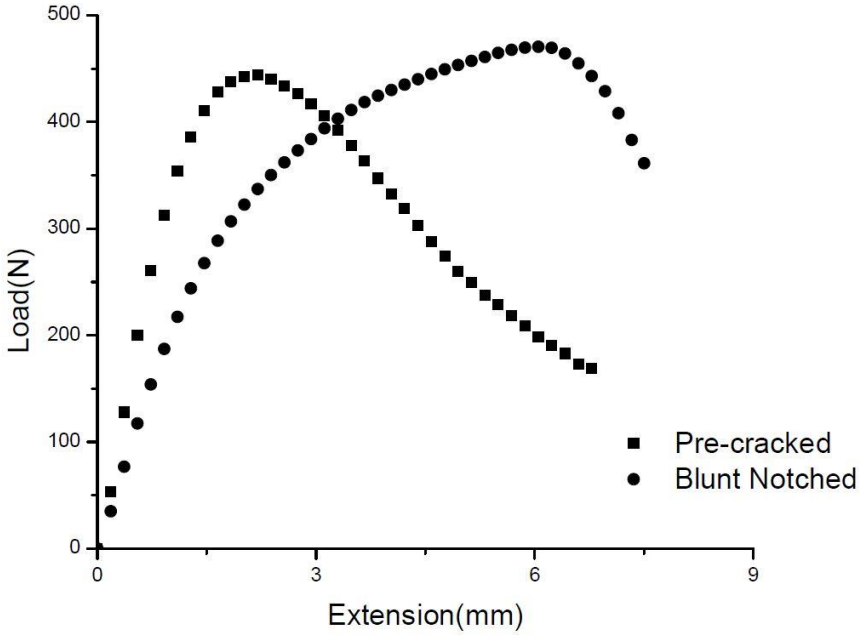

Figure 22: Load curve of the large sized, pre-cracked and blunt notched specimens of unaged PVDF A with a/W=50 % tested with crosshead speed of 10 mm/min.

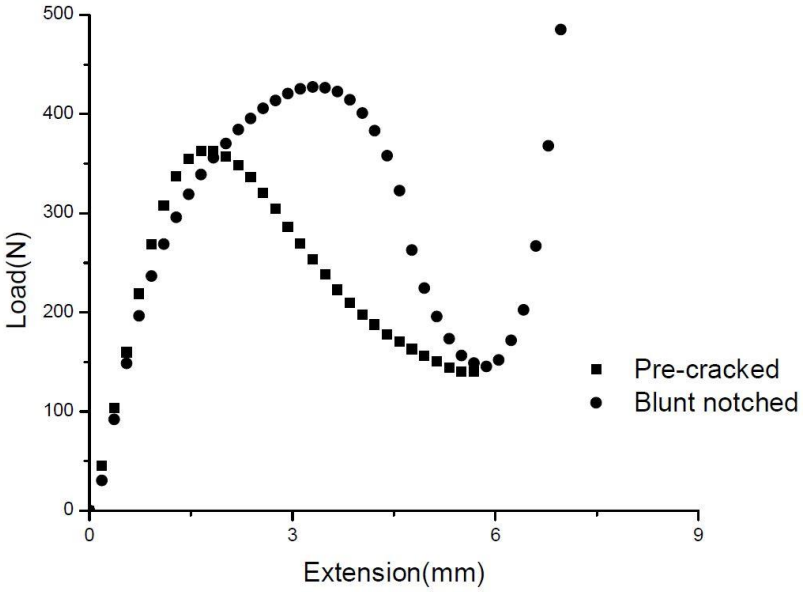

Figure 23: Load curves of the medium sized, specimens of unaged PVDF A with a/W=50 % tested with crosshead speed of 10 mm/min.

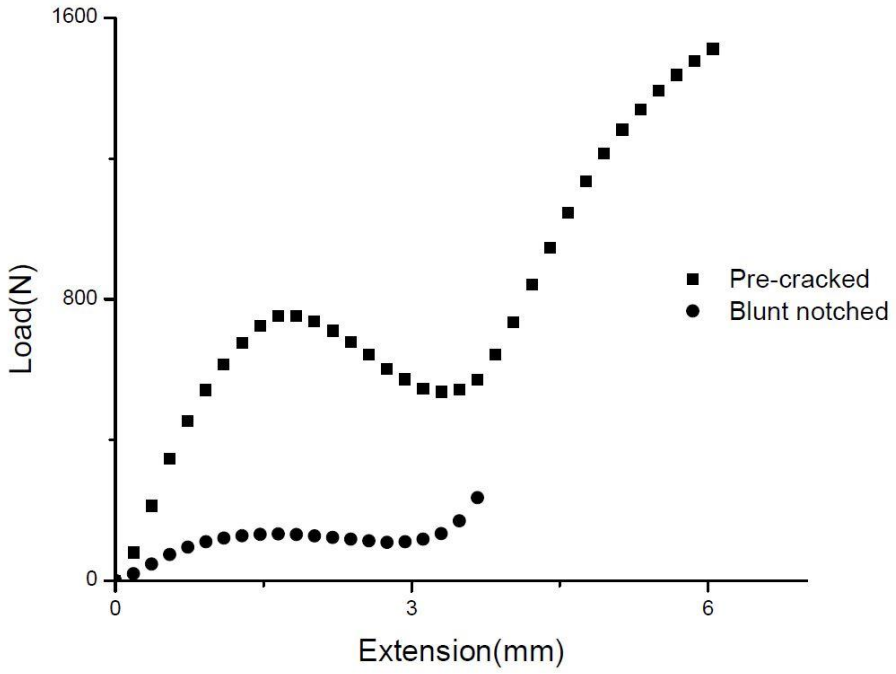

Figure 24: Load curves of the small sized specimens of unaged PVDF A with a/W=50 % tested with crosshead speed of 10 mm/min.

Comparing these curves, it is suggested that large specimens present greater loads than the medium. However, the same cannot be said regarding the smallest.

There are 2 points worth noting on this method: is the data regarding the blunt notched specimen must cover a larger displacement than the one regarding the pre-cracked specimen; and when comparing specimens with different initial crack length, only the plastic displacement is to be considered. When specimen with the same geometry and material are compared, this latter point is not relevant since the elastic region is going to be mostly the same. In order to guarantee first point, the blunt notched specimen is tested first to determine the maximum displacement we have to apply to the pre-cracked.

Also, the curves in Figures 22 and 23 show that the blunt notch leads to maximum loads greater than the pre-crack. This effect is expected, since the pre-crack concentrates stress a lot more, due to its tip curvature. Other than that, it is also worth noting that greater crack or blunt notch depths led to smaller loads. This is due to the fact that a bigger initial

crack length requires a smaller applied stress to grow. This was not seen in the curves related to the small sized specimens. This is due to the fact that the load was not applied only in the crack tip, but also in the region in contact with the supports. This phenomenon is called Compression Jamming. This leads to interference in the load measure due to it being applied to different regions other than the crack and makes the test data not valid. This happens with the small and medium specimens because of their very small size compared to the rolls. This also seem to have happened at the very end of the tests using the medium sized specimen. However, it only happened after the crack started propagating and, therefore, did not affect the results we are looking for, which is the beginning of the crack propagation.

At last, in these curves, we can also observe the effects of the loading rate on the crack growth. In figure 25 curves from tests done with different rates can be seen. Both tests were done two identical specimens. They were large, blunt notched specimen made of PVDF A and had a crack depth of a/W= 50 %. Tests done with higher rate presented slightly larger loads. Both had the same initial crack length and were tested until the same crosshead displacement. From these curves, it is possible to note that the specimen tested with a higher crosshead speed shows a slightly higher maximum load. The PVDF A tested with higher speed showed significant crack growth, while the one tested with lower speed didn't present visible crack growth. This behavior is due to the viscoelasticity of polymeric materials. When a higher test rate is applied to a polymeric material, it displays a more elastic behavior, rather than viscous. This translates into a higher material strength, but lower ductility. In the case of the fracture test, this can be seen as a higher maximum load that occurs at a lower displacement.

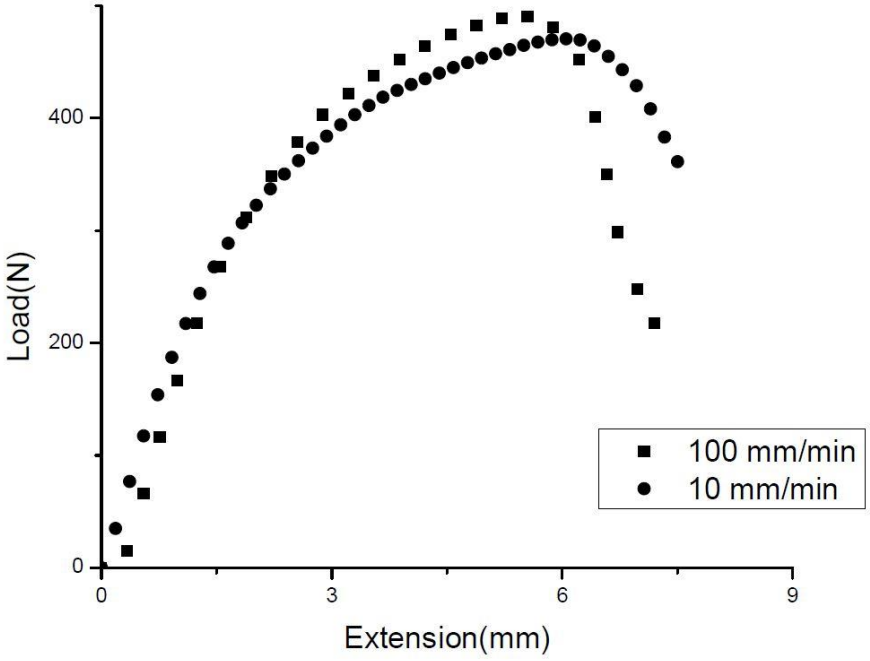

Figure 25: Tests done on large blunt notched specimens of unaged PVDF A with a/W=50 % at 2 different rates: 10 mm/min and 100 mm/min.

In the figure 26 there are load-displacement curves of the medium sized specimen made of aged PVDF A. In these curves, it can be observed that the aged material reached a higher load than the unaged one (see figure 23), which is to be expected since the aging process lead to an increase in the material's crystallinity. This increase in maximum load can suggest a higher fracture toughness than the unaged PVDF A.

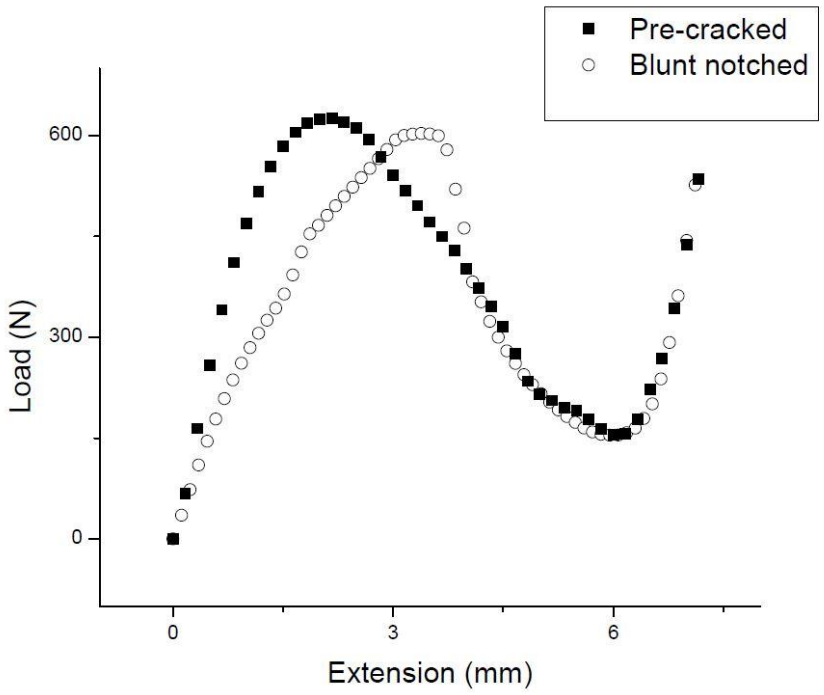

Figure 26: Load-displacement curves of medium sized aged PVDF A specimens.

The load-displacement curves of the small specimens, regardless of the material, a second, sudden increase in load after the falling. This mostly doesn't happen with the other. This probably happens because the roll applying the load is too big for this geometry, which, again, lead to compression jamming. So, since the load is not being applied to the crack, the S_{pb} method cannot be applied to this geometry because the intrinsic S_{pb} factor does not keep constant, as required. In fact, the load was majorly applied tin the support region on this type of specimen and much higher loads than expected were observed.

The figure 17 is an example of the processed images from the fracture tests that will be analyzed in a DIC software. Based on this technique, the deformation fields were determined.

Using the nCorr software to analyze the processed images, it is possible to create the displacement map of the surface. In figure 27 is the initial displacement map of a medium specimen of PVDF A. The variability in the displacement is due to noise in the analysis. In figure 28 is the frame in which the displacement fields became greater around the pre-crack

with a gradient towards the ends of the specimen. This aspect is kept through the rest of the test, with the displacements becoming greater.

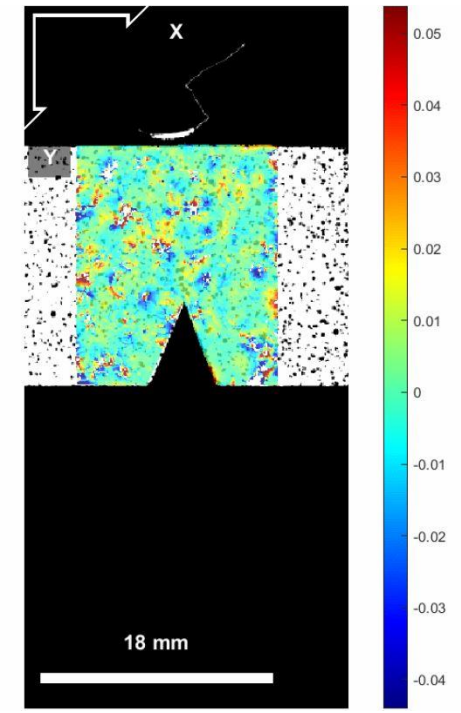

Figure 27: Starting image in the DIC analysis.

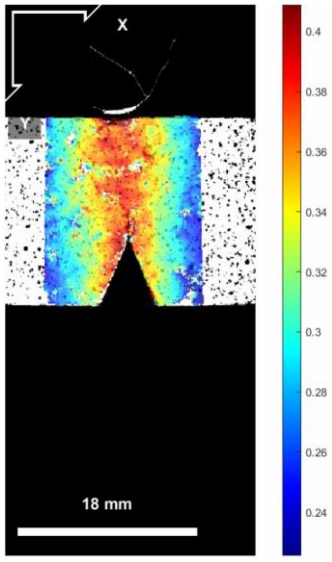

Figure 28: Displacement field localized around the pre-crack.

In the red region, as it can be seen in the field map bar, there is the greatest strain. In this image, this is around the pre-crack. Using the software Ecorr lab, which is the software

responsible for capturing the images, each frame was related to a test time, crosshead displacement and load. Using this relation, each image can be related to a point in the S_{pb} curve, and therefore, we can verify if the crack started, in fact, growing in this point. According to the data collected, this frame is taken after 8.2 s of test. After this period of time, the crosshead displacement is 0.822 mm and the load is 241.4 N.

Due to the ability to relate each image with the test time, it is possible to relate the displacement field, created through the DIC, and the point in the load-displacement curve, created with the data processed by the software Blue Hill 3. With this, it is possible to analyze the displacement field in different load levels. This is seen in figure 29 and 30. In figure 29, the load-displacement curve made from the fracture test done with a crosshead speed of 10mm/min to the large sized pre-cracked specimen with a crack depth of 50 % made of unaged PVDF A. And in figure 30, it is a load-displacement curve made from the fracture test done with the same conditions as the previous one, but with a medium sized specimen.

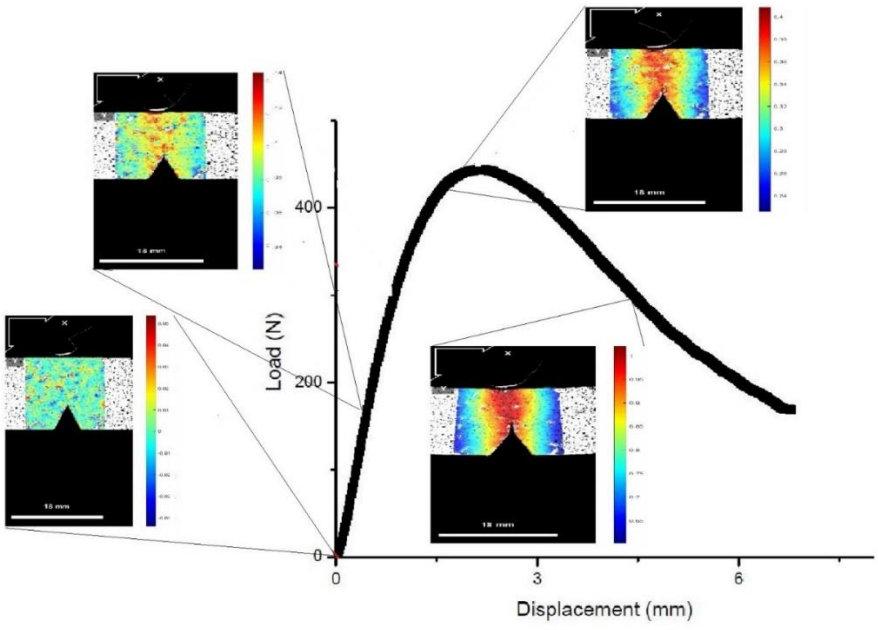

Figure 29: Load-displacement curve of a fracture test done to a large unaged PVDF A specimen with crack depth of a/W=50 %, with a displacement field corresponding to each region of the curve.

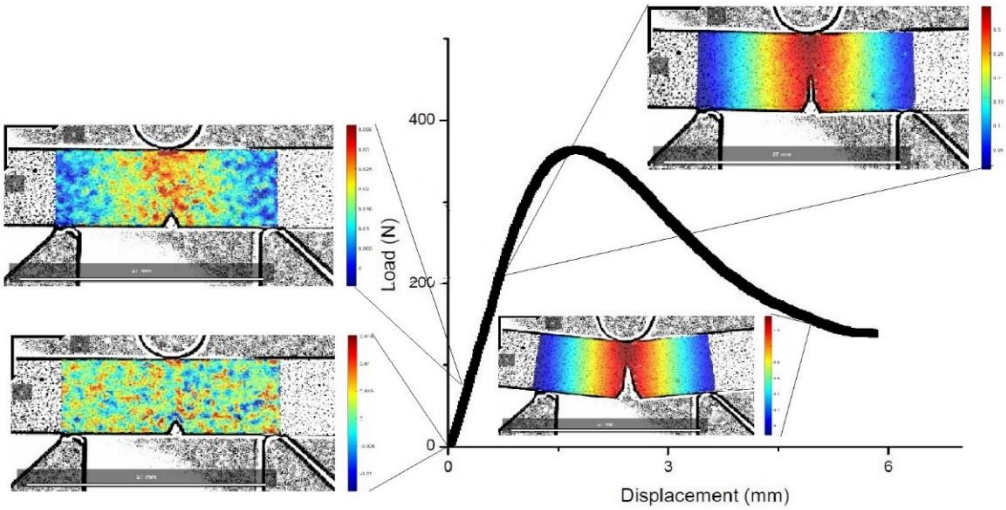

Figure 30: Load-displacement curve of a fracture test done to a medium sized unaged PVDF A specimen with a/W=50 %, with a displacement field corresponding to each region of the curve.

4.3. S_{PB} Method

The method studied is based on the S_{Pb} factor which is based on the load separation principle, that is, the consideration that the load is a product of 2 factors: a geometric function and a deformation function. The S_{Pb} separation factor is the ratio between the load between a pre-cracked specimen and a blunt notched one and it is independent of the deformation factor of the material. So, any changes to this factor are due to changes in geometry, or more specifically, changes to the crack size. It is assumed that the fall is due to the crack growth [15].

The load separation principle, as said before, assumes that the load, *P*, is the product of 2 functions: G, which depends only on the geometry, and H, which depends only on the material's properties, as could be seen in Equation 5 [16].

The specimens compared to use this method, then, have to present the same geometry, material and constraint. [15].

Since the specimen pre-cracked with a blade presents a crack with a much smaller radius than the blunt notched specimen, the crack growth starts in it first. This results in the decrease of its load and of the S_{Pb} factor. So, this means, in theory, that the fall in the S_{Pb} factor indicates the moment the crack starts to grow.

The firsts tests made were fracture tests in the blunt notched specimen of both materials. This was done to verify if the load separation is valid for these materials. In order to do so, from the tests, the ratio S_{bb}, which is the ratio between two blunt notched specimens with different initial crack length, is calculated. The 2 under script b indicates that the factor is the ration between 2 blunt notched specimens. For these tests, the specimens were blunt notched following the same procedure as before but reaching with a/W=60 % and 70 %, instead of 40 % and 50 %. The S_{bb} factor can be seen in figure 31.

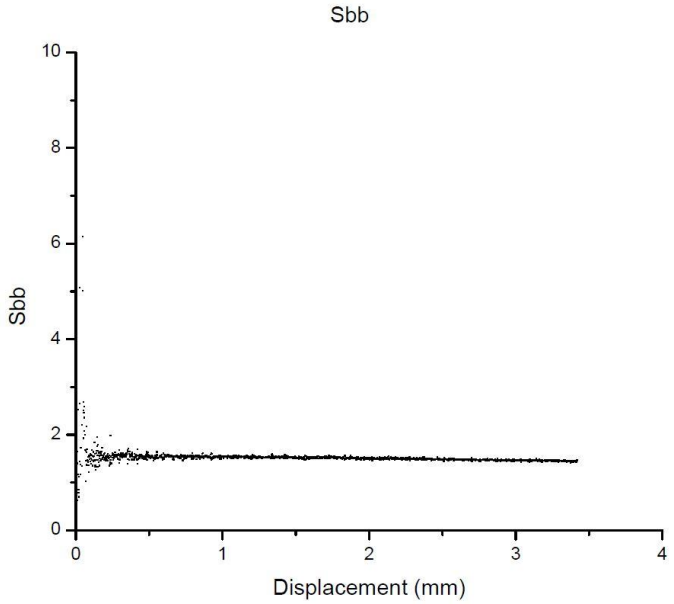

Figure 31: S_{bb} factor between two blunt notched specimens of PVDF A, one with a/W=60 % and the other with a/W=70 %.

In figure 31, 2 regions can be seen: an unstable initial region and a constant second region, which goes on until the end of the test. The unstable initial region corresponds to the elastic region. If this result were to be used to determine the J integral, this region would not be considered. The constant behavior indicates that the material is following the ration given by Equation 1. This indicates the material is obeying Equation 1 and, therefore, the load separation principle is applicable to this material and the S_{Pb} method can be used.

In figures 32 and 33, the typical S_{Pb} factor-displacement curves for a crosshead speed of 10 mm/min and 100 mm/min, respectively, can be seen. The DIC images of the pre-cracked specimen in different instants in the S_{Pb} curves are shown.

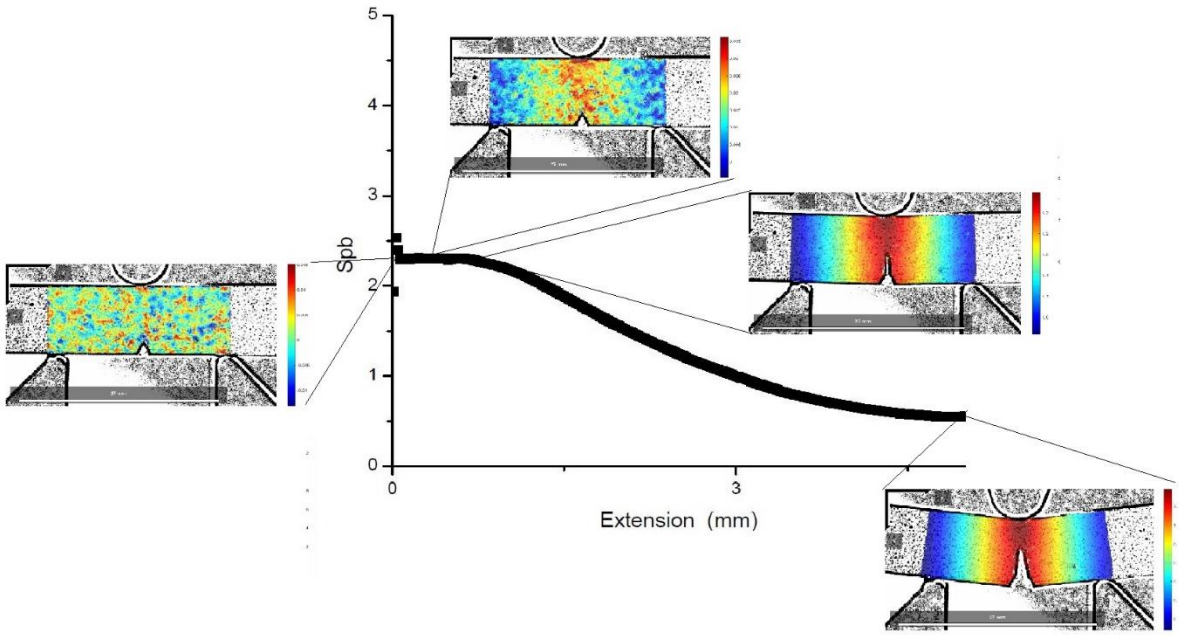

Figure 32: Typical S_{Pb} curve of the unaged medium PVDF A specimen with a/W=50% with crosshead speed of 10 mm/min, with the correspondent displacement field in different regions of the curve.

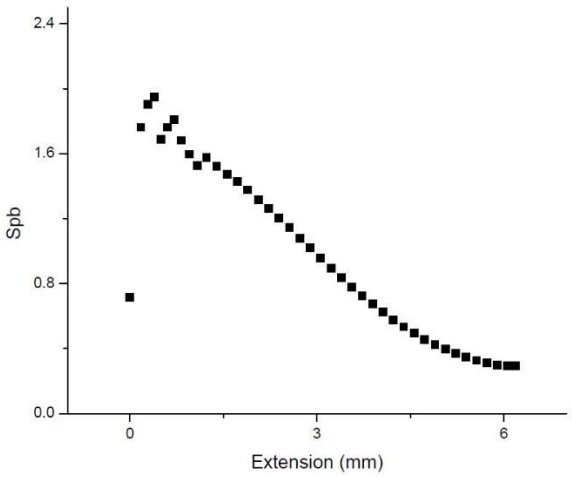

Figure 33: Typical S_{Pb} curve of the unaged medium PVDF A specimen with crosshead speed of 100 mm/min.

The curves were made only to the specimen with medium and large geometries because, as it was said before, this method cannot be applied to the small specimen due to the compression jamming. However, only the large specimen data may be reliable, since the medium specimen also displayed compression jamming, even if it is only showed in the curve at the end of the test. Based on the curves, the crosshead displacement that makes the crack start to grow is determined. The curves from the fracture tests with other conditions and from the fractures tests done with PVDF B.

From these curves, it is possible to observe the effects of loading rate and the geometry on the material's fracture toughness. Specimen with a bigger geometry present a S_{Pb} falling point with greater displacement, indicating that the crack started growing at a higher crosshead displacement than the medium ones.

The S_{Pb} curves made for the PVDF B follow the same trend as the ones above, with slightly different values. This means that PVDF B, when tested with crosshead speed of 10 mm/min displays a constant region followed by a fall off region, while when it was tested with a crosshead speed of 100 mm/min, this is not the case. These curves can be seen in the annex.

As it can be seen in figure 33, the S_{Pb} curve of PVDF A doesn't follow the trend required to use this method when the loading rate applied is 100 mm/min, while this is not true when it is 10 mm/min. This difference in properties is probably due to the viscoelasticity, which is intrinsic to the polymeric materials. The higher crosshead speed leads to a much higher loading rate, due to the small size of the crack tip radius. This leads to different mechanical behaviors when different crosshead speed and this is probably the reason why in one condition the material displays the load separation principle, while in another condition it does not. This happens in both PVDF A and B. Since they do not present the required constant region in the S_{pb} curve when the loading rate is 100 mm/min, we can conclude that this method cannot be applied to these materials under these conditions. This may be due to the fact that the higher crosshead speed made the crack in the blunt notched specimen grow. Since this crack size was not kept constant during the test, S_{pb} method cannot be used in this condition. In figure 34, an image of a large, blunt notched specimen made of unaged PVDF A tested with crosshead speed of 100 mm/min is shown. A prominent white line grown from the hole can be seen. That line is a crack that grew from the hole during the test.

Figure 34: Large, blunt notched specimen made of unaged PVDF A after being tested with crosshead speed of 100 mm/min.

At last, in figure 35 are the curves of aged and unaged medium sized specimen with crack size of 50 % of depth. These curves allows us to make a comparison between PVDF A before and after the annealing. The annealing made the S_{Pb} factor fall off in a smaller displacement. This is due to the effect that annealing process has on the material's crystallinity as the increase observed in the DSC tests. This change made the material to present higher fracture toughness, as the load-displacement curves suggest, but a smaller displacement was needed to induce the growth of the pre-crack.

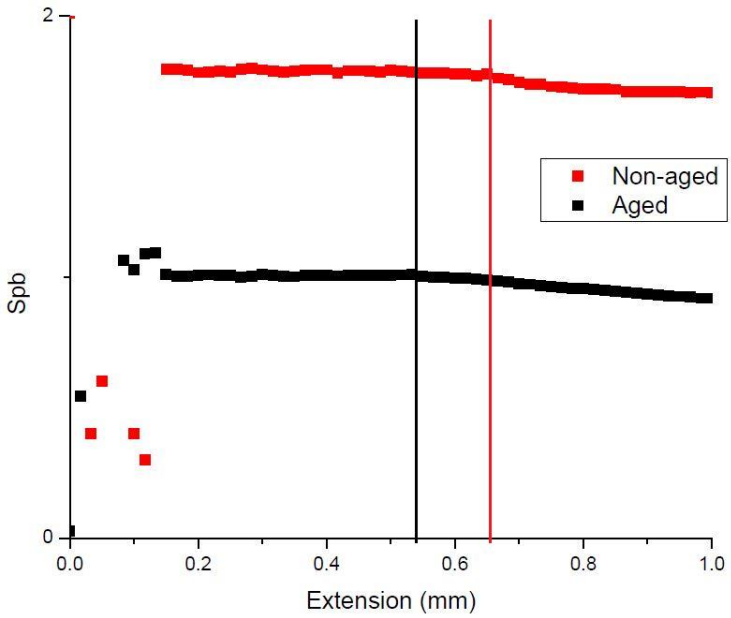

Figure 35: Comparison between the S_{pb} factor of an aged and an unaged medium sized PVDF A specimen.

The change in crystallinity caused changes in the mechanical properties, as it can be seen in the tensile tests as well as in the fracture tests. The increase in the fraction of crystalline phase makes annealed PVDF A to present a higher maximum load than the unaged PVDF A, but a smaller displacement until the crack growth, as it can be seen in the S_{Pb} curves, where the annealed specimens showed crack growth at smaller displacements, as it can be seen in table 1. This is due to the fact that the polymer's crystalline phase has few sliding systems, causing it to have few plastic deformation mechanisms and less ductility

due to the loss of the amorphous phase, a combination that lead to the crack propagating with a smaller crosshead displacement [9].

Table 1: Comparison of relevant observed values of the different pre-cracked specimens obtained from tests done with crosshead speed of 10 mm/min.

Material	Geometry	a/W	Maximum Load (N)	S_{pb} displacement (mm)
Unaged PVDF A	Large	40 %	444.1	1.70
Unaged PVDF A	Large	50 %	434.4	1.51
Unaged PVDF A	Medium	40 %	363.9	0.63
Unaged PVDF A	Medium	50 %	357.8	0.56
Aged PVDF A	Medium	50 %	625.5	0.5
PVDF B	Large	40 %	577.7	1.69
PVDF B	Medium	40 %	564.9	0.75
PVDF B	Medium	50 %	423.5	0.65

Besides determining the moment the crack growth starts, the S_{Pb} factor method also allows to determine the pre-cracked specimen's crack size based on the blunt notched crack size. It is also done based on the ratio between their loads. This is done based on the Equation 10 [14]:

$$a_p = a_b \times {S_{pb}}^{\frac{1}{\eta}} = a_b \times (\frac{P_p}{P_b})^{\frac{1}{\eta}} \quad (10)$$

Even though the crack growth started at a lower displacement after the aging process, the loads it reached were around 50 % greater, as it can be seen when comparing the load-displacement curves in the figure 23 and 26, while the difference in displacement is around 10 %, as it can be seen in the comparison between the S_{Pb} curves in figure 34.

4.4. Fracture Surface

An image of a tested sample taken in the microscope can be seen in figure 36. The red color is caused by the dye penetrant applied beforehand. This image was taken with a magnification of 10x and it clearly shows the extent of the crack growth during the test. The holes in the middle of both halves of the specimen is also an interesting observation and it motivated the use of the SEM, for a more thorough investigation. The aspect of the images taken from PVDF A and B didn't show any noticeable difference. The crosshead speed did not show any effect on the aspect of the fracture surface, as well.

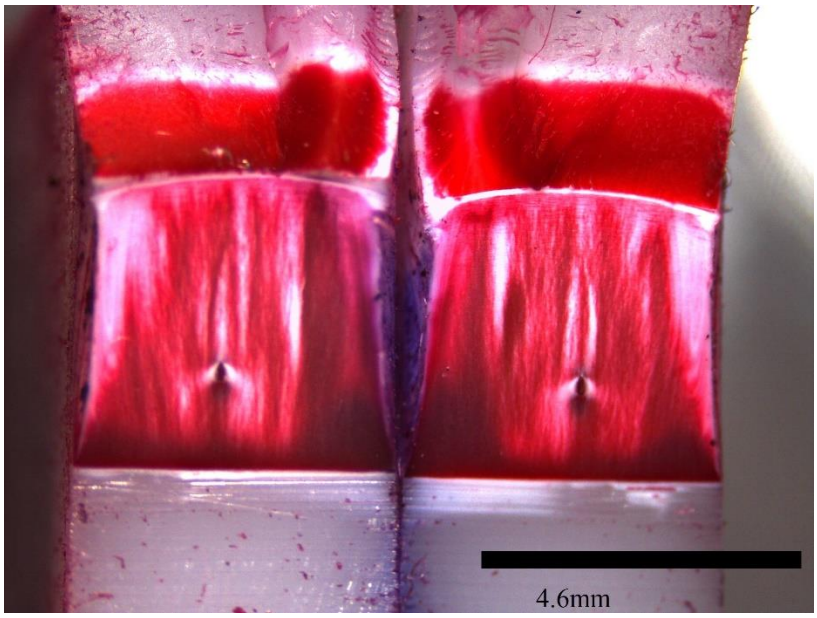

Figure 36: Fracture surface of a medium sized PVDF B specimen with dye penetrant applied and with 10x magnification.

In figure 37, a SEM image taken from the fracture surface of the PVDF B. The cavity seen in figure 36 is greatly magnified, 100x, however it was not yet identified. One interesting feature this image displays is the small roughness of the fracture surface. In figure 38, another image of the same specimen can be seen, but in another region of the fracture surface. It can be noticed that the surface is not displaying any signs of plastic deformation, suggesting that the crack grew through brittle mechanisms.

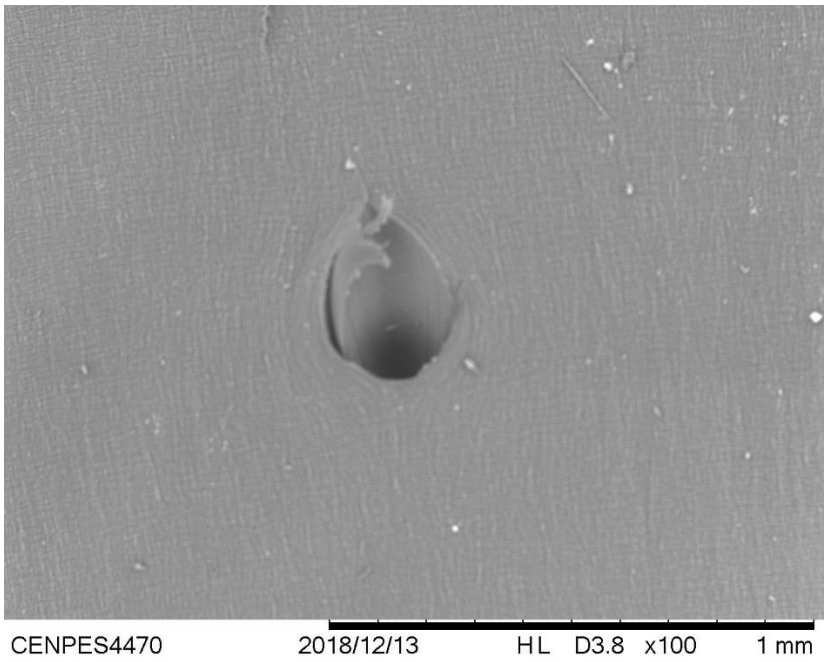

Figure 37: SEM image of a tested large sized PVDF B specimen, with 100x magnification.

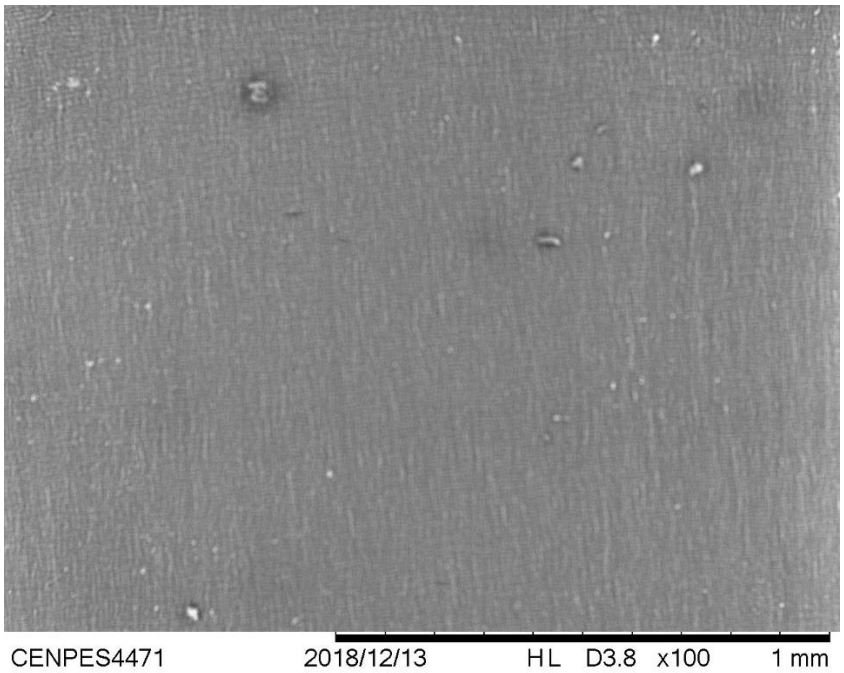

Figure 38: SEM image of a tested large sized PVDF B specimen, with 100x magnification.

First, it was thought that this hole was due to the presence of the polyethylene in it. However, as it was seen in the study done by Marlon Demauir Cozine Silva, the polyethylene spheres have a radius smaller than 5 μm, while the hole seen in the SEM image show a radius of almost 1 mm, invalidating this hypothesis [19].

Since this feature is displayed by both materials, regardless of the crosshead speed, and only in some specimen, it is believed that this cavity might be due to some problem during the processing, more specifically the extrusion that was only revealed due to the nature of the fracture test.

5. Conclusions

Through fracture tests done in different conditions, it was possible to conclude that the S_{pb} method can be applied to both commercial grades of PVDF when the crosshead speed is 10 mm/min, but when a speed of 100 mm/min is used, this is no longer the case.

Also, the DSC tests showed that the annealing process resulted in an increase of crystallinity and this change is seen in the maximum load observed in the fracture tests, as well as in the S_{Pb} curves. In the case of the fracture tests, the annealed specimens showed a much higher maximum load than the unaged ones. Also, when the S_{pb} method was applied, only a slight decrease in the displacement needed to cause the crack propagation is observed. This suggests that, even though the annealed material fractures at a lower displacement, it possesses a higher fracture toughness, due to the overall increase of total energy required to cause the crack propagation, which can be interpreted as the area under the curve in the load-displacement curve until the point of crack growth.

With the use of the DIC technique, it was possible to observe different displacement field patterns in different regions of the load-displacement field: when no load is applied, before the crack propagates, and after the crack starts growing. This was observed in both large and medium geometries. After the start of the crack propagation, the displacement

field shows a very distinct pattern of a highly localized displacement around the pre-crack, which is to be expected due to the nature of the test.

At last, through the observation of SEM images of the fracture surface, it is possible to observe that both crosshead speeds of 10 mm/min and 100 mm/min caused fracture in a brittle mode. This is indicated by the lack of any signs of ductility in the fracture surface of the specimen.

6. References

[1] Young, R. J. and Lovell, P. A. *Introduction to Polymers*, 2 ed., Hong Kong, Springer-Science Business Media, 1991.

[2] Anderson, T. L, *Fracture Mechanics: Fundamentals and Applications*, 3 ed., New York, CRC Press, 2005.

[3] Wypych, G., *Handbook of Polymers*, Toronto, ChemTec Publishing, 2016.

[4] Li, X., Jiang, X., and Hopman, H., “A review on predicting critical collapse pressure of flexible risers for ultra-deep oil and gas production”, *Appl. Ocean Res.*, vol. 80, pp. 1–10 June, 2018.

[5] Canevarolo, S. V, *Ciência dos Polímeros*, São Paulo, Artliber LTDA, 2006.

[6] Banerjee, S., *Handbook of specialty fluorinated polymers: preparation, properties and applications*, Pennsylvania, Elsevier, 2015.

[7] Ward, I. M., Sweeney, J., *The Mechanical Properties of Solid Polymers*, 2 ed., Chichester, Wiley, 2004.

[8] Lucas, E. F.,Soares, B. G., Monteiro, E. E. C., *Caracterização de Polímeros: Determinação de Peso Molecular e Análise Térmica*. E-papers, 2001.

[9] Bowden, P. B., Young R. J., “Review Deformation mechanisms in crystalline polymers”, *J. Mater. Sci.*, vol. 9, pp. 2034–2051, 1974.

[10] Thomas, C., Seguela, R., Detrez, F.,Miri,V., Vanmansart, C., “Plastic deformation of

spherulitic semi-crystalline polymers: An in situ AFM study of polybutene under tensile drawing," *Polymer (Guildf).*, vol. 50, no. 15, pp. 3714–3723, 2009.

[11] Roux, S, Réthoré, J., Hild, F., "Digital image correlation and fracture: An advanced technique for estimating stress intensity factors of 2D and 3D cracks," *J. Phys. D. Appl. Phys.*, vol. 42, no. 21, 2009.

[12] Reu, P. L., Wellman, G. W., Rogillio, B. R., "Stable Crack Growth Measurement using DIC as a Tool for Model Validation," no. Dic, 2007.

[13] Janssen, M., Zuidema, J., Russell, W., *Fracture Mechanics*, 2 Edi., Delft, DUP Blue Print, 2002.

[14] Wainstein, J., Frontini, P. M., Cassanelli, A. N., "J-R curve determination using the load separation parameter Spbmethod for ductile polymers," *Polym. Test.*, vol. 23, no. 5, pp. 591–598, 2004.

[15] Rodríguez, C., Maspoch, M. L., Belzunce, F. J., "Fracture characterization of ductile polymers through methods based on load separation," *Polym. Test.*, vol. 28, no. 2, pp. 204–208, 2009

[16] Baldi, F., Agnelli, S., Riccò, T., "On the applicability of the load separation criterion in determining the fracture resistance (JIc) of ductile polymers at low and high loading rates," *Int. J. Fract.*, vol. 165, no. 1, pp. 105–119, 2010.

[17] Frontini, P. M., Fasce, L. A., Rueda,F. , "Non linear fracture mechanics of polymers: Load Separation and Normalization methods," *Eng. Fract. Mech.*, vol. 79, pp. 389–414, 2012.

[18] Bernal, C. R., Cassanelli, A. N., Frontini, P. M., "A simple method for J-R curve determination in ABS polymers," *Polym. Test.*, vol. 14, no. 1, pp. 85–96, 1995.

[19] Silva, M. D. C., "Geração do Efeito Whitening em Polifluoreto de Vinilideno(PVDF) sob Carregamento Cíclico," Universidade Federal do Rio de Janeiro, 2014.

Annex

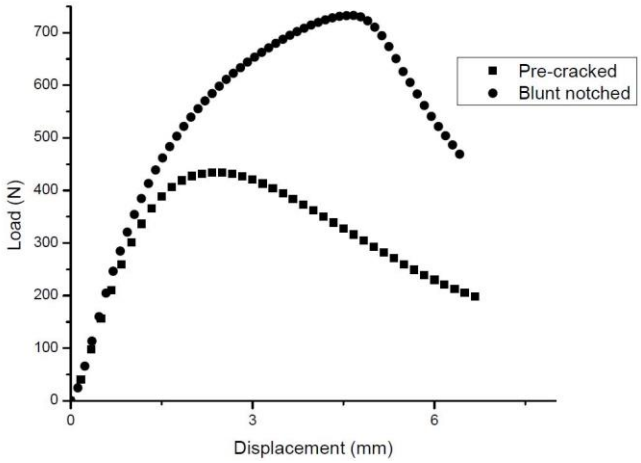

Figure 38: Load-displacement curves obtained from a fracture test with crosshead speed of 10 mm/min performed with large and unaged PVDF A specimens. They both had a crack depth of 40%.

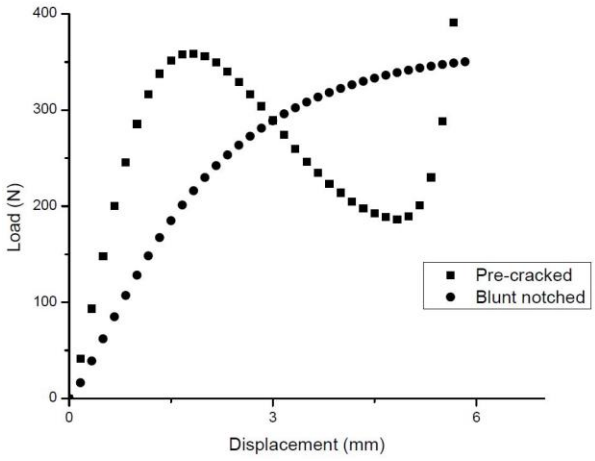

Figure 39: Load-displacement curves obtained from a fracture test with crosshead speed of 10 mm/min performed with medium and unaged PVDF A specimens. They both had a crack depth of 40%.

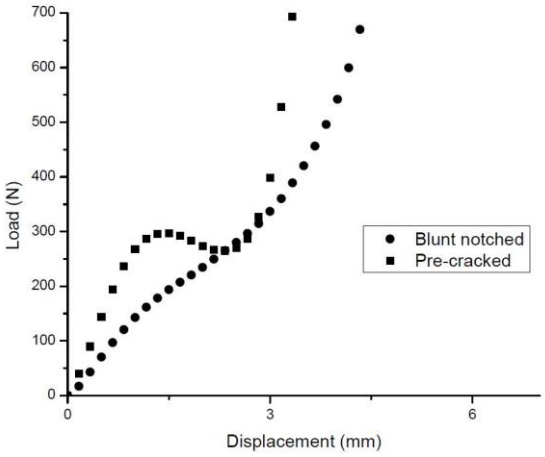

Figure 40: Load-displacement curves obtained from a fracture test with crosshead speed of 10 mm/min performed with small and unaged PVDF A specimens. They both had a crack depth of 40%.

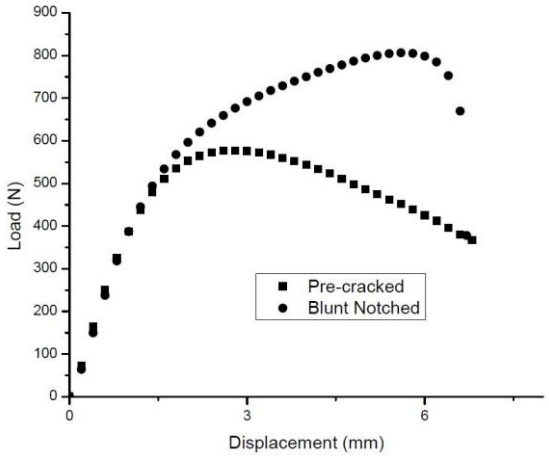

Figure 41: Load-displacement curves obtained from a fracture test with crosshead speed of 10 mm/min performed with medium PVDF B specimens. They both had a crack depth of 40%.

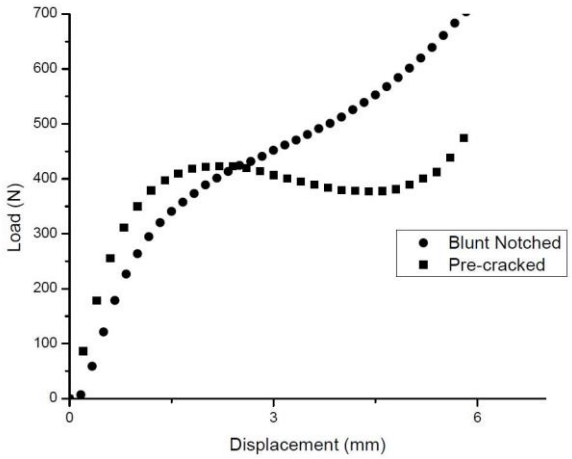

Figure 42: Load-displacement curves obtained from a fracture test with crosshead speed of 10 mm/min performed with medium PVDF B specimens. They both had a crack depth of 50%.

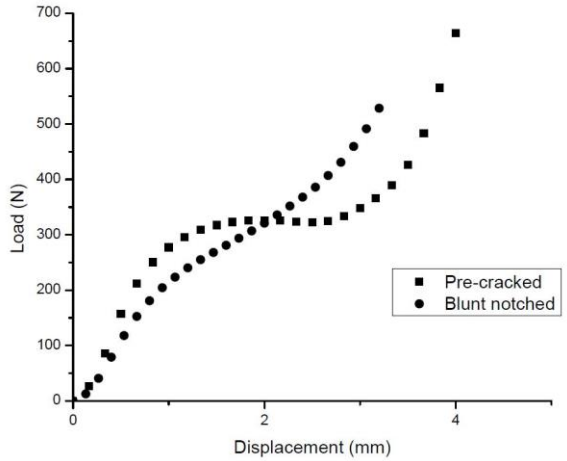

Figure 43: Load-displacement curves obtained from a fracture test with crosshead speed of 10 mm/min performed with small PVDF B specimens. They both had a crack depth of 40%.

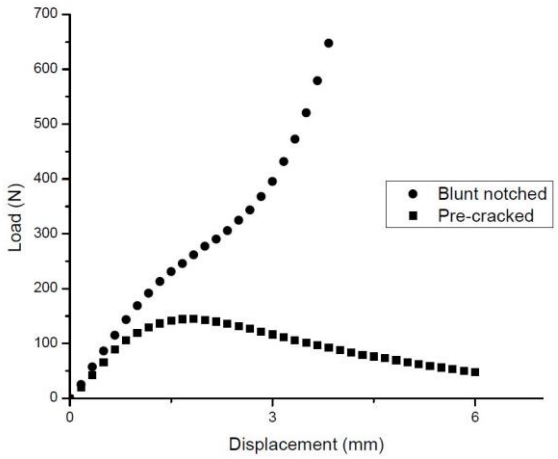

Figure 44: Load-displacement curves obtained from a fracture test with crosshead speed of 10 mm/min performed with small PVDF B specimens. They both had a crack depth of 50%.

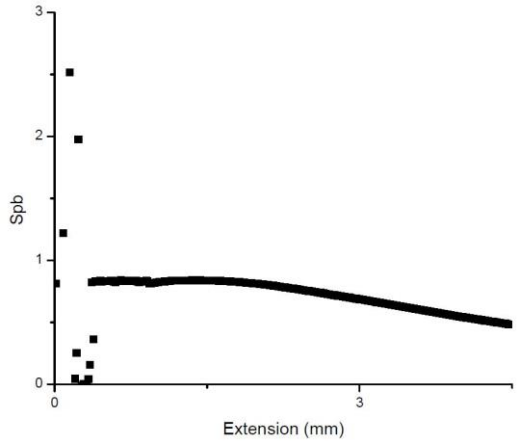

Figure 45: S_{pb} curve of large, unaged PVDF A specimens with crack depth of 40% tested with crosshead speed of 10 mm/min.

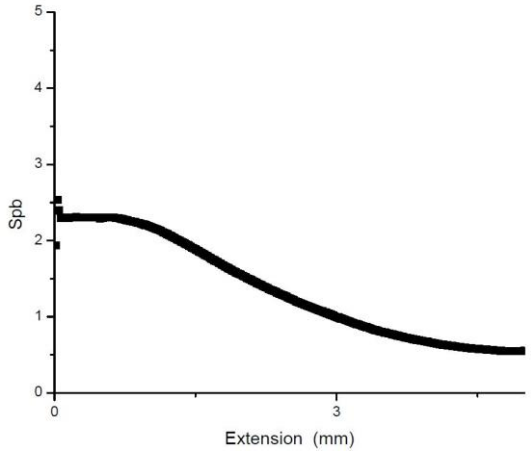

Figure 46: S_{pb} curve of medium sized, unaged PVDF A specimens with crack depth of 40% tested with crosshead speed of 10 mm/min.

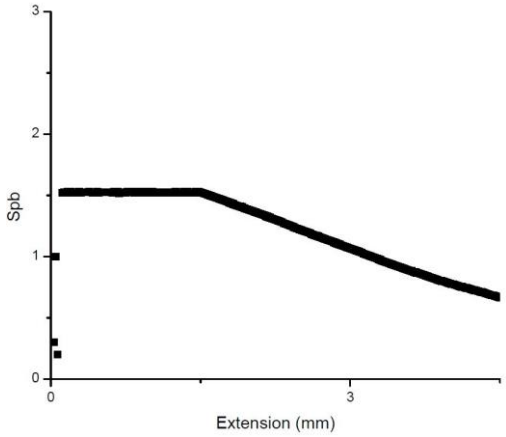

Figure 47: S_{pb} curve of large, unaged PVDF A specimens with crack depth of 50% tested with crosshead speed of 10 mm/min.

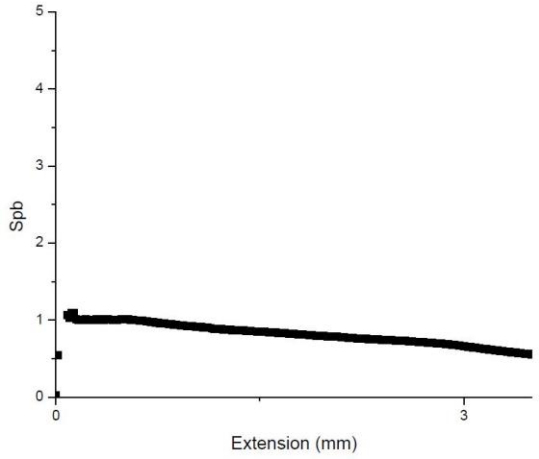

Figure 48: S_{pb} curve of medium, unaged PVDF A specimens with crack depth of 50% tested with crosshead speed of 10 mm/min.

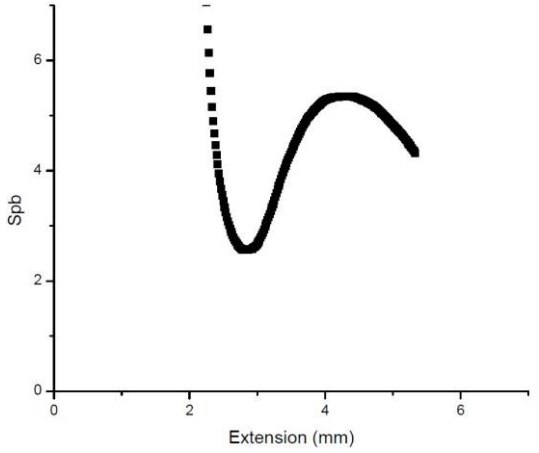

Figure 49: S_{pb} curve of small, unaged PVDF A specimens with crack depth of 50% tested with crosshead speed of 10 mm/min.

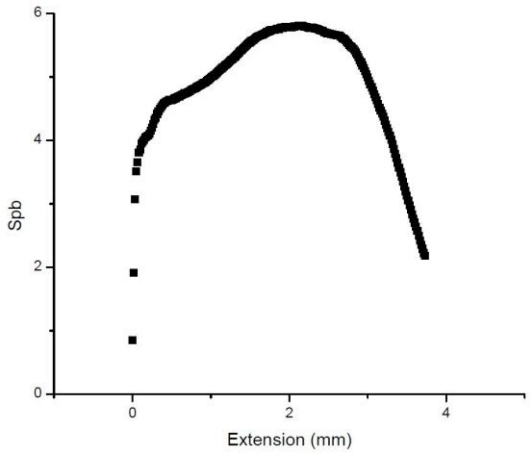

Figure 50: S_{pb} curve of small, unaged PVDF A specimens with crack depth of 40% tested with crosshead speed of 10 mm/min.

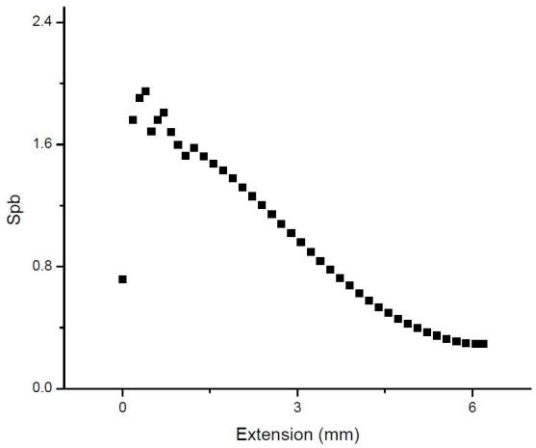

Figure 51: S_{pb} curve of large, unaged PVDF A specimens with crack depth of 50% tested with crosshead speed of 100 mm/min.

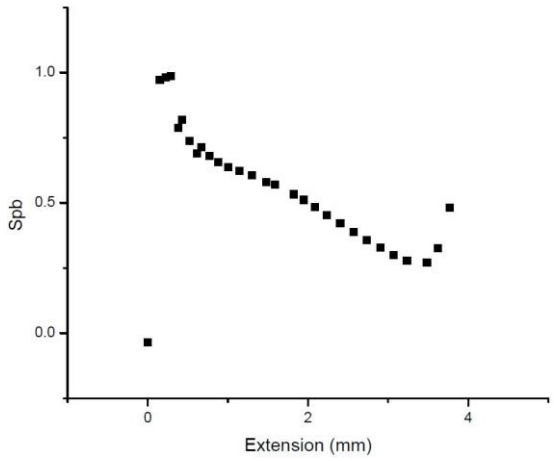

Figure 52: S_{pb} curve of medium, unaged PVDF A specimens with crack depth of 40% tested with crosshead speed of 100 mm/min.

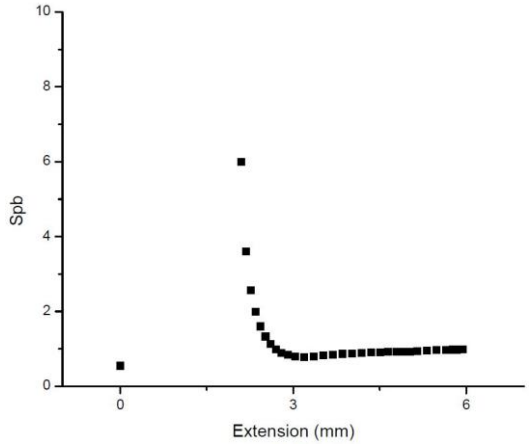

Figure 53: S_{pb} curve of small, unaged PVDF A specimens with crack depth of 40% tested with crosshead speed of 100 mm/min.

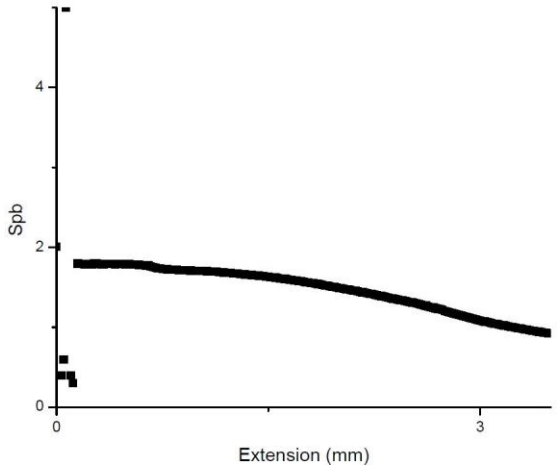

Figure 54: S_{pb} curve of medium, annealed PVDF A specimens with crack depth of 50% tested with crosshead speed of 10 mm/min.

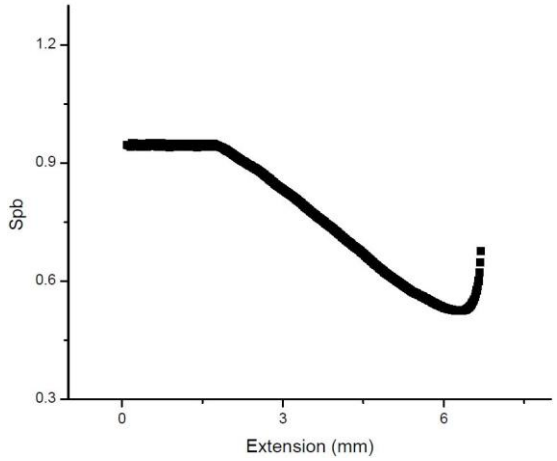

Figure 55: S_{pb} curve of large PVDF B specimens with crack depth of 40% tested with crosshead speed of 10 mm/min.

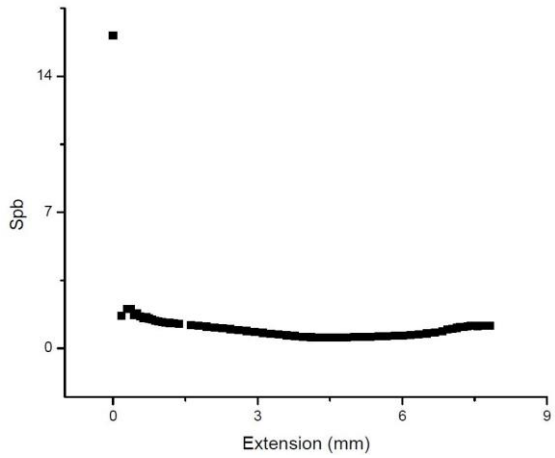

Figure 56: S_{pb} curve of medium PVDF B specimens with crack depth of 40% tested with crosshead speed of 100 mm/min.

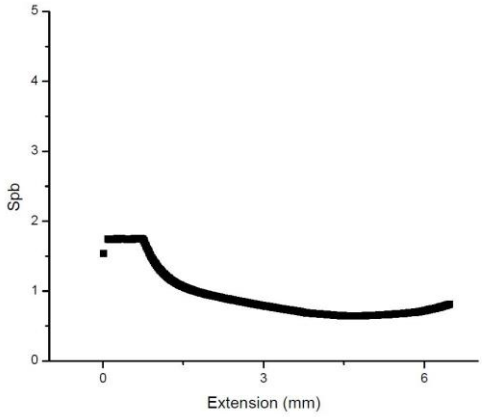

Figure 57: S_{pb} curve of medium PVDF B specimens with crack depth of 40% tested with crosshead speed of 10 mm/min.

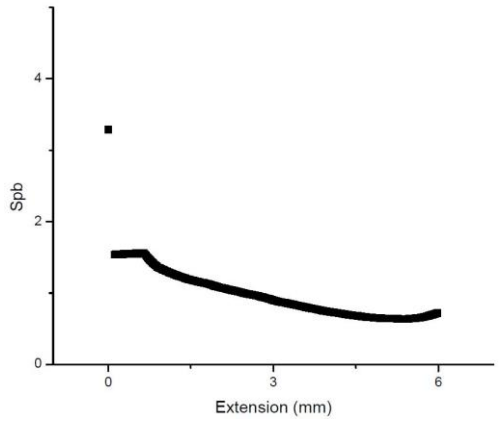

Figure 58: S_{pb} curve of medium PVDF B specimens with crack depth of 50% tested with crosshead speed of 10 mm/min.

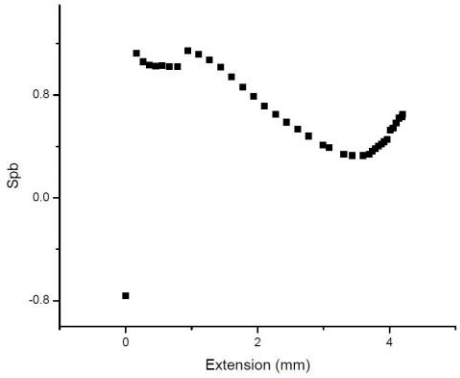

Figure 59: S_{pb} curve of small PVDF B specimens with crack depth of 50% tested with crosshead speed of 10 mm/min.

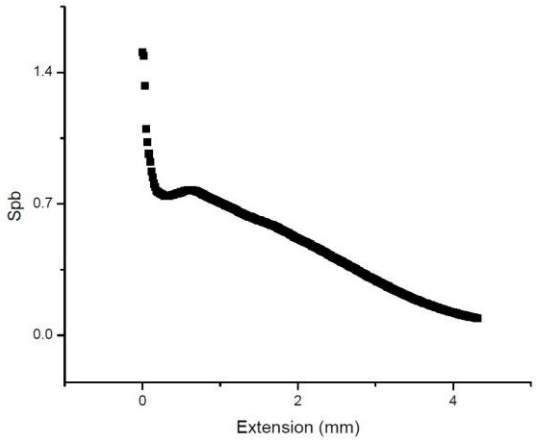

Figure 60: S_{pb} curve of small PVDF B specimens with crack depth of 50% tested with crosshead speed of 100 mm/min.